



Review

Lithium-Sulfur Batteries: Advances and Trends

Claudia V. Lopez, Charini P. Maladeniya and Rhett C. Smith *

Department of Chemistry, Clemson University, Clemson, SC 29634, USA; cvlopez@g.clemson.edu (C.V.L.); cmalade@g.clemson.edu (C.P.M.)

* Correspondence: rhett@clemson.edu

Received: 21 April 2020; Accepted: 5 June 2020; Published: 1 July 2020



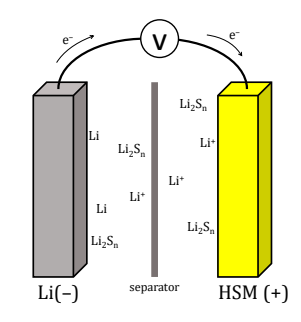
Abstract: A review with 132 references. Societal and regulatory pressures are pushing industry towards more sustainable energy sources, such as solar and wind power, while the growing popularity of portable cordless electronic devices continues. These trends necessitate the ability to store large amounts of power efficiently in rechargeable batteries that should also be affordable and long-lasting. Lithium-sulfur (Li-S) batteries have recently gained renewed interest for their potential low cost and high energy density, potentially over 2600 Wh kg⁻¹. The current review will detail the most recent advances in early 2020. The focus will be on reports published since the last review on Li-S batteries. This review is meant to be helpful for beginners as well as useful for those doing research in the field, and will delineate some of the cutting-edge adaptations of many avenues that are being pursued to improve the performance and safety of Li-S batteries.

Keywords: lithium-sulfur batteries; polysulfide; cathode materials; high sulfur materials

1. Introduction

1.1. General Operation of Lithium-Sulfur (Li-S) Batteries

Lithium-sulfur (Li-S) batteries have emerged as preeminent future battery technologies in large part due to their impressive theoretical specific energy density of 2600 W h kg⁻¹. This is nearly five times the theoretical energy density of lithium-ion batteries that have found widespread market penetration in applications where high power output is needed in portable consumer devices such as hand-held electronics and cordless power tools. Discharge in Li-S batteries occurs according to the two-stage process shown in Scheme 1A, so that the most simplistic Li-S battery is configured as shown in Scheme 1B. When Li-S batteries were first described, the cathode material was simply elemental sulfur. More modern configurations have been improved by replacing elemental sulfur with high sulfur-content materials (HSMs) and supported cathode structures that are more mechanically robust and can be chemically tuned.



(A) $S_8 + 2e^- + 2 \operatorname{Li}^+ \rightarrow \operatorname{Li}_2 S_8$ $\operatorname{Li}_2 S_8 \rightarrow \operatorname{Li}_2 S_8 + (8-n) S \quad (B)$

Scheme 1. Discharge reactions in Li-S Batteries (**A**) allows Li ions to be shuttled between electrodes as represented in the highly simplified diagram (**B**). HSM = high sulfur-content material, which could even be elemental sulfur.

1.2. Summary of Recent Reviews on Li-S Batteries

The promise of Li-S batteries has led to the publication of several excellent reviews in the last five years. In this section, the topics of those previous reviews will be summarized so that the interested reader may find more detail in those references. The area of perhaps the most emphasis has been on developing advanced cathode materials [1–7]. The solubility and localization or mobility of Li_2S_n in contemporary organic electrolytes used in these batteries remains a significant barrier to Li-S battery development as well [8–12]. As Li_2S_n is solubilized, cathode mass erodes, with attendant loss of capacity and poor cycling stability. There is also a need to attenuate reaction of polysulfides and lithium anode materials, and to prevent dendrite growth at the anode interface [13–17]. The role of polysulfides and the shuttling mechanism have been independently reviewed in some detail [18–20]. Some efforts to replace the organic polyelectrolytes with more aqueous-based systems, gels [12] or solid-state materials [9,21–24], in which polysulfide solubility may be attenuated and the chemistry changed to a great extent while still providing promising performance, have been explored as potential improvements [25].

Other avenues to electrode additives and sulfur host compounds or implementation of added components to the simplified design (current collectors, interlayers, functionality-added separators, etc.) have also been discussed critically [26]. The lithium anode can also be modified with surface chemistry to protect it from the shuttle of polysulfide species and to stabilize their interface with electrolytes [4,13,21,22,24,26–35].

Several reviews also center on the origin and nanoscale architecture of the materials used in the Li-S battery material. For example, metal organic frameworks (MOFs) have been used to exploit the tunable composition and pore structure to serve as elements themselves or to template other materials [2,36,37]. Biomass has been explored as a sustainable alternative to synthetic or petrochemical-derived materials, wherein biomass often has added benefits of high adsorption properties and affordability [38,39].

More work on fully understanding the nuances of how Li-S batteries work on the molecular level will undoubtedly facilitate the rational design of next-generation concepts for Li-S batteries. The sophisticated spectroscopic methods and new techniques that are under active development to probe these mechanisms will contribute to these endeavors [19], as will advanced redox kinetic studies [40]. The current review discusses only work reported in the time since the last review article was published. The metrics for the Li-S batteries discussed herein are summarized in Table 1.

Table 1. Summary of lithium-sulfur (Li-S) battery metrics.

Entry	Battery Attributes	Coulombic Efficiency (%)	After How Many Cycles?	Charge Density (C)	Discharge Capacity (mAh g^{-1})	Ref.
		99.6	1400	-	-	
1	Li@carbon nanofiber anode	83.6	200	0.5	1.0	[41]
	_	-	=	4	350	
2	Vanadium nitride support for both cathode and anode	99.6	850	4	-	[42]
3	Solid state mesoporous carbon/sulfur cathode	-	200	0.1	1150	[43]
		-	200	0.2	727	[10]
4	Sulfur cathode and a gel polymer electrolyte and a layer of pentaerythritol tetrakis divinyl adipate	85	300	2	-	[12]
5	Carboxylate and sulfonate micelles (affinity for polysulfides)	96.8	100	0.5	571	[44]
6	Ultrathin separator (double hydroxide nanosheets, graphene oxide and a polypropylene)	-	-	0.2	1090	[45]
	Carbon nanofiber layer in cathode, surface terminated with Mo and C nanotubes	-	-	0.1	1401	[46]
7		70	500	1	-	
	(higher cathode loading of $7.64~\mathrm{mg~cm^{-2}}$)	-	100	0.2	-	
8	${\rm Li_2S_6}$ catholyte is hosted by a carboxyl-modified graphene oxide sponge			0.1	1607	[47]
Ü		87	200	1	_	
	Carbon-nanotubes and Prussian blue nanocrystals as cathode support	74	200	0.2	1200 to 1457	
9		61	500	0.5		[48]
	Initial capacity without the C nanotubes	-	-	-	500	
10	Fe ₂ O ₃ nanoparticles in multi-walled carbon nanotubes	-	500	1	545	[49]
10	(MWCNTs) cathode			7	340	
11	Three-dimensional porous material of MoS ₂ nanotubes with	-	200	0.2	1219	[50]
11	n-doped graphene sheets	96.1	500	1		
12		-	-		1485	
	Porous interlayer of carbon microfibers	-	200	0.2	615	[51]
		-	-	1	600	
13	Phosphorus and nitrogen co-doped into the carbon	-	-	-	900	[52]
13	(sulfur loading of 3.5 mg cm $^{-2}$)	84	450	0.2	-	

 Table 1. Cont.

Entry	Battery Attributes	Coulombic Efficiency (%)	After How Many Cycles?	Charge Density (C)	Discharge Capacity (mAh g^{-1})	Ref.
14	N-doped carbon hollow spheres SnS ₂ nanoparticles on exterior (sulfur loading of about 3 mg cm ⁻²)	-		0.2	1344	[53]
14		-	200	0.5		
15	Double-shelled hollow polyhedron of nitrogen-doped carbon nanodots (Co-NC@Co ₉ S ₈ /NPC)	98.9	2000	2	-	[54]
13	(sulfur loading 4.5 mg cm ⁻²)		500			
16	Infusion of sulfur into hollow pore carbon structures	56	1000	-	-	[55]
17	Nitrogen-doped carbon nanotubes in tandem with metallic cobalt nanoparticles	60	500	1	-	[56]
17	Performance of prior systems using N-doped	20	500	-	-	
18	B,N co-doped C nanotube with Co nanoparticles as sulfur host for cathode	-	200	0.1	1160	[57]
10		84.8	400	1	1008	[07]
19	Cells with phosphorous/oxygen co-doped into mesoporous carbon bowls – (sulfur loading of 5.02 mg cm ⁻²)	-	-	1	897	[58]
1)		52	800	-	489	
20	Sb ₂ Se _{3-x} as a polysulfide barrier in sulfur electrochemical conversion	86.5	500	1	-	[59]
21	Cathode assembly involving co-melting of sulfur and selenium	-	100	-	800	[60]
22	Inorganic separators comprising anodized aluminum oxide membranes	49.6	480	2	-	[61]
23	Graphdiyne nanosheets on polypropylene as a separator _	-	- 0.1	1262	[62]	
25		-	500	1	412	[02]
24	Poly(sulfur-co-1-vinyl-3-allylimidazolium bromide as a cathode	90	900	-	-	[63]
25	${\rm MnO_2}$ nanoparticles embedded in polyaniline (PANI) as a scaffold for sulfur cathode	-	100	0.5	1195	[64]
25		-	500	2	640	
26	Cathode conductivity using polypyrrole and tin oxide nanoparticles	75	500	1	-	[65]
		90	-	5	383.7	
27	Mesoporous silica framework with polypyrrole having NiO nanoparticles in it	-	300	-	700	[66]
28	a polymer-encapsulated sulfur cathode	74	600	2	-	[67]

 Table 1. Cont.

Entry	Battery Attributes	Coulombic Efficiency (%)	After How Many Cycles?	Charge Density (C)	Discharge Capacity (mAh g^{-1})	Ref.
	Polypropylene as a scaffold for a polysulfide-blocking	-	-	-	938	
29	separator layer	60	500	1	-	[68]
	High sulfur loading (3.2 mg cm^{-2})	-	100	0.5	601.3	
30	Gelatin-carbon nanofiber interlayers with high sulfur loading at the cathode (9.4 mg $\rm cm^{-2}$)	-	100	0.1	-	[69]
31	Carbon nanofibers interlayer with konjac glucomannan _	-	-	0.2	1286	[70]
01		84	400	1	-	
	Sodium alginate derivative affinity laminated chromatography membrane layers	-	-	0.1	1492	[71]
32		76	200	0.2	-	
32	high-loading electrodes	-	-	0.05	1302	
		95.2	40	0.1	-	
33	Separator made of urea and amylose in the presence of nickel chloride with high cathode loading (7 mg cm ⁻²)	95.7	100	4	714	[72]
34	Polymeric zwitterion interlayer	88	1000	-	-	[73]
34		-	300	-	-	
35	Oxygen content influence in corncob with sulfur composite cathode	-	-	-	1504	[74]
33		-	200	0.3	799	r1
36	Sulfurized polyacrylonitrile with C nanotubes and conductive CoS_2 cathode with sulfur loading of (5.9 mg cm ⁻²)	-	-	-	1322	[75]
37	Carbon nitride as components of a metal organic framework (MOF) that served as a separator layer	88	12,000	0.2	1532.1	[52]
37				1.0/2.0	1000	[02]
20	Nitrogen doped into MOF as cathode	86	500	1	-	[52]
38				5	600	[32]
39	Ultrathin sheets of MOF	58	600	-	641	[52]
40	MOF utilized carbon cloth, graphene nanocloth, and cobalt phosphide components grown on graphene	- 85	- 500	3 2	930.1	[52]
40	(sulfur at a loading of 2 mg cm ⁻²) (higher sulfur loadings of up to 10.83 mg cm ⁻²)			0.05	813.5	
41	Nitrogen-rich MOF as cathode with iron nanoparticles	-	-	0.2	1123	[52]
41		70	500	-	605	[32]

 Table 1. Cont.

Entry	Battery Attributes	Coulombic Efficiency (%)	After How Many Cycles?	Charge Density (C)	Discharge Capacity (mAh g ⁻¹)	Ref.
42	CoMn ₂ O ₄ microspheres as sulfur hosts in the cathode	-	=	-	524.3	[52]
43	Lithium sulfide in a three-dimensional mesoporous carbon architecture	-	-	0.1	848	[52]
			400	2	410	[32]
44	Hollow spheres of titanium oxide and titanium nitride	99	500	-	1254	[52]
45	ZIF-67 fiber material (conjunction with cobalt nanoparticles and dicyandiamides)		100	0.1	867.44	[76]
46	ZIF-67 framework (Li $_2$ S $_6$ containing catholyte current collector) (high sulfur loading of 4.74 mg/cm $^{-2}$)		300	0.2	1166 938 910	[77]
	(sulfur loading 7.11 mg/cm ⁻²)				910	
47	Co_3S_4/MnS nanotubes(sulfur loading of 3.2 g cm ⁻²)	95	200		-	[78,79]
48	Ni ₃ S ₂ fabricated into a N/S-doped reduced graphene oxide	77	1000	3	1158.6	[80]
49	One hollow architecture comprising a combination of zinc sulfide and iron sulfide encapsulated in a nitrogen doped carbon structure			4	718	[81,82]
1)			200	0.2	822	[01/02
50	MnS-nanofiber interlayer(sulfur loading of 2 mg cm ⁻²)		400	1	714	[83]
50			100	0.5	894	[00]
51	Ruthenium- Mo_4P_3 nanoparticles on carbon nanospheres (high sulfur loading of up to 6.6 mg cm ⁻²)		50	0.5 4	1178 660	[84]
52	Ni ₂ Co ₄ P ₃ species (sulfur loading of 25 mg cm ⁻²)			0.1	1223	[85]

2. Anode and Anode Interface Design

Most recent work on Li-S batteries has focused on cathode materials and separators. Comparably few efforts have sought to modify or replace the Li anode, despite the risk of safety hazards and catastrophic failure a device may suffer if uncontrollable dendritic growth occurs from the electrode [36,37]. One study attempted to replace the lithium metal electrode with a lithium@nanofiber roll composite electrode [41]. The result was a series of hollow carbon structures wherein lithium is disposed to reside (Figure 1). Over 1400 cycles, Li-S batteries made with this electrode showed impressive 99.6% coulombic efficiency. This study is of note because most studies focus on separator layers and cathode configurations, while a stable anode is also essential for safely performing consumer device. More work should be undertaken in the near future on Li-host anodes. It would also be intriguing to see how a cell would perform if this anode were combined with some of the more successful separator layers or cathode morphologies discussed herein. Such combinations are prime candidates for future studies.

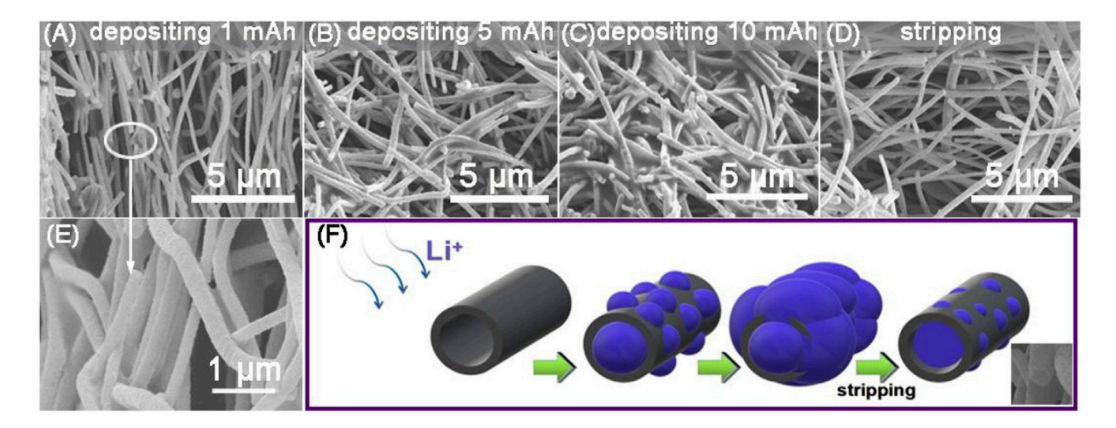


Figure 1. Scanning electron microscope (SEM) images of carbon nanofibers as Li is deposited (**A–C,E**) or stripped (**D**), a process shown schematically in the inset (**F**). Reprinted from reference [41], © 2020 used with permission from Elsevier.

Another way to combat the safety hazards of flammable organic electrolytes in combination with dendrite-prone lithium anodes is to make the electrolyte itself flame-retardant. One such effort employed as electrolyte DME/TFSI (dimethoxyether/1,1,2,2-tetrafluoroethyl 2,2,3,3-tetrafluoropropyl ether) [86] in conjunction with a non-woven cellulose coated with non-conductive carbon as a separator layer (Figure 2). This electrolyte proved quite flame retardant and to simultaneously support low polysulfide solubility. From a performance standpoint a Li-S battery employing these elements exhibited good long term cycling stability for over 2500 h at 1.0 mA cm $^{-2}$ and 1.0 mAh cm $^{-2}$. When this electrolyte is used in conjunction with a bare sulfur cathode for 200 cycles at 0.5 C, it retains 83.6% of its discharge capacity. At higher charge density (4 C) a capacity of 350 mAh g $^{-1}$ is possible. The authors also tested the cell at elevated temperature and found that at 60 °C discharge capacity of 870 mAh g $^{-1}$ is possible. These flame-retardant electrolytes could be an excellent means of addressing the concern some have over the safety of Li batteries.

In an effort to address both the shuttle effect and the potential for lithium to engage in dendrite growth, one study employed a vanadium nitride nanowire array to support both a sulfur cathode and a lithium metal anode (Figure 3) [42]. These vanadium nitride nanowires are exceedingly conductive and provide a high surface area. Vanadium nitride also proved highly efficient in trapping polysulfides, facilitate so high ion in electron transport through the material answer ports good redox kinetics. Notably, this configuration successfully inhibits lithium dendrite growth even at a remarkably high current density of 10 mA cm⁻² after over 200 h of repeated plating/stripping. The cell has a high areal capacity of 4.6 mAh cm⁻² while over 850 cycles it also maintains high coulombic efficiency (\approx 99.6% at 4

C). Given the superior performance of the vanadium nitride system, the testing of other carbon-free supports in Li-S batteries is clearly a top priority for future studies.

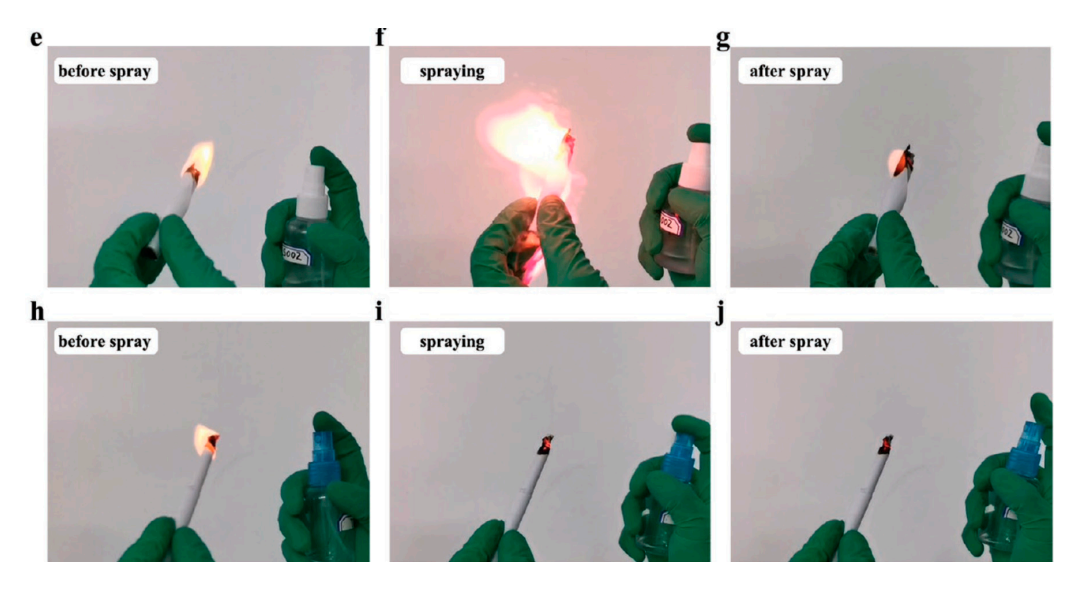


Figure 2. A flaming piece of paper is monitored as it is sprayed with a traditional organic electrolyte (**e**−**g**) or with the flame-retardant electrolyte dimethoxyether/1,1,2,2-tetrafluoroethyl 2,2,3,3-tetrafluoropropyl ether (DME/TFSI) (**h**−**j**). Reprinted from reference [86], © 2020 used with permission from John Wiley and Sons.

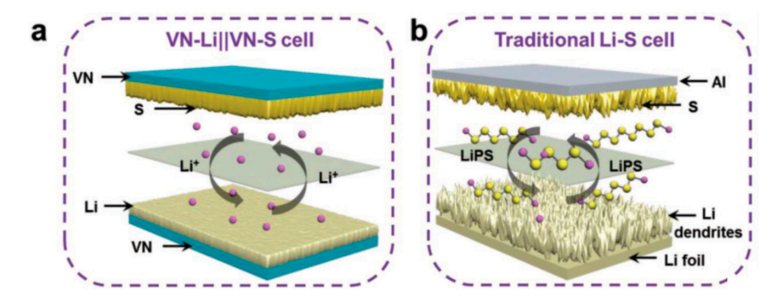


Figure 3. Comparison of the vanadium nitride-supported cell (**a**) to the traditional Li-S cell (**b**). Reprinted from reference [42], © 2020 used with permission from John Wiley and Sons.

3. Electrolyte Design

3.1. Solid-State Electrolytes

One strategy bent on attenuating the polysulfide shuttle issue in solution is to employ sulfide solid-state electrolytes (SSEs) [9,21–24], an approach that will likewise attenuate the possibility of Li battery fires fueled by flammable organic electrolytes. A recent study employing simulation using density functional theory (DFT) and ab initio molecular dynamics has sought to understand processes by which the cathode and SSE interface with S_8 or Li_2S (Figure 4) [87]. The authors specifically explored β -Li₃PS₄, Li₆PS₅Cl, and Li₇P₂S₈I, as these materials have demonstrated superionic conductivity of Li⁺. The simulations provide some insight into adhesion and interfacial energy for these materials, allowing for some speculation on the mechanisms of interfacial reactions. These simulations should be followed up with experiments and imaging techniques in an effort to validate them and, if the simulations prove predictive, further simulations will guide additional work in the field.

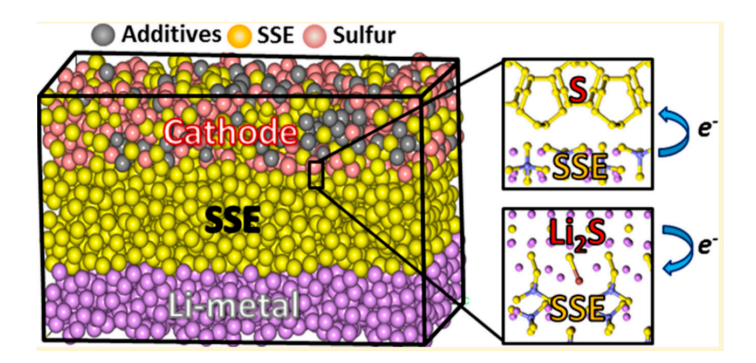


Figure 4. Interfacial interactions between solid-state electrolytes (SSEs) and either S8 or Li2S provide insight into electron transport in their composite Li-S batteries. Reprinted with permission from reference [87]. Copyright 2020 American Chemical Society.

A potential issue holding back the development of solid state electrolytes is that they generally have poor kinetics compared to solution systems. An interesting approach to improving the kinetics is to add a eutectic accelerator. In one case, tellurium was employed in this role [43]. The solid electrolyte interface was set up on a mesoporous carbon (CMK-3)/sulfur cathode. Tellurium doping (1 wt %) was observed to improve diffusion kinetics and produces a solid electrolyte interface with high lithium ion conductivity and low impedance. After 200 cycles, the cell had a high reversible specific capacities of 1150 mAh $\rm g^{-1}$ and 727 mAh $\rm g^{-1}$ at 0.1 C and 0.2 C, respectively. This study illustrates an effective strategy for improving kinetics in solid state electrolyte cells that have inherently low shuttle effects.

3.2. Polymer and Gel Electrolytes and Electrolyte Carriers

One source of shuttle problems is the solubility of polysulfides and related species in the organic electrolytes of traditional Li-S batteries. One potential solution to this issue is to use a polymerized or polymer gel electrolyte [12]. For example, a Li-S battery comprising a sulfur cathode and a gel polymer electrolyte of poly(ethyleneoxide)-modified poly(vinylidene fluoride-co-hexafluoropropylene) (PEO-PVDF) was fabricated in which a layer of pentaerythritol tetrakis (divinyladipate) was further added to suppress polysulfide permeability (Figure 5) [88]. These polymers were selected because they are known to exhibit high thermal stability and low thermal expansion, as well as their permeability and ion conductivity potential. The battery so composed featured a porous membrane that could take up 280% by mass of electrolyte, resulting in an ionic conductivity of 9.6×10^{-4} S cm⁻¹ and a lithium cation Li⁺ transference number of 0.71 at 25 °C. The coulombic efficiency remains near quantitative over 300 cycles with retention over 85% capacity even after 300 cycles at 2 C.

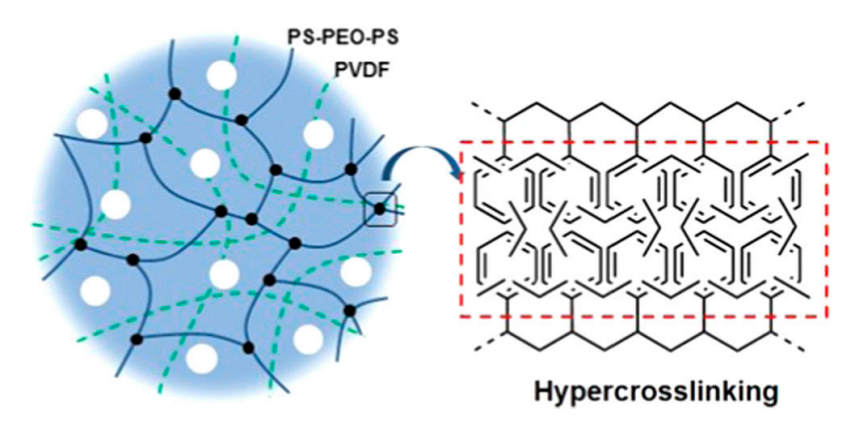


Figure 5. A highly crosslinked network provides a scaffold that resists dimensional changes in response to temperature. Reprinted with permission from reference [88]. Copyright 2020 American Chemical Society.

Organic polymers can also be incorporated into batteries in the form of crosslinked micelles that can also carry electrolyte. In one such illustration [44], a copolymer of polyethylene oxide and polypropylene oxide comprising carboxylate and sulfonate groups was used to form the micelles (Figure 6) wherein lithium polysulfides (LiPS) are envisioned to interact along the polar polymer chains. These highly polar and ionic polymer segments, as expected, have a very high affinity for LiPS. Cells having this polymer micelle binder exhibited a reversible capacity of 571 mAh $\rm g^{-1}$ and, over 100 cycles at 0.5 C, showed a capacity loss of only 0.032%/cycle. These new polymer micelle-containing cells outperform older technologies such as Li-S batteries comprising fluoropolymer components, while also being safer to fabricate and more environmentally friendly.

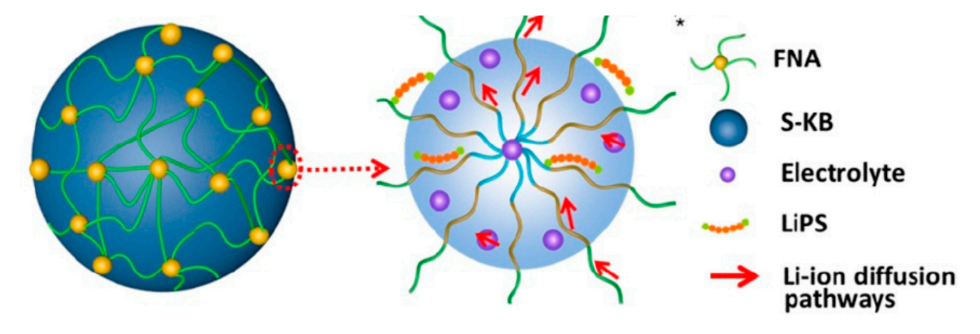


Figure 6. A series of crosslinked micelles (left; green tubes are polymer chains; yellow spheres are micelles) provide a template for lithium polysulfide (LiPS) interaction with polymer chains as they approach the electrolyte entrapped in the micelle. Reprinted with permission from reference [44]. Copyright 2020 John Wiley and Sons.

The merits of an ultrathin separator having a width of only about 30 nm were employed to confine about a 1 nm active space through the use of a double hydroxide nanosheets, graphene oxide and a polypropylene layer-by-layer assembly (Figure 7) [45]. This assembly effectively blocked polysulfides while facilitating dispersion of Li $^+$. Li-S batteries having this separator layer indeed show a high initial discharge capacity of 1092 mAh g $^{-1}$ while only exhibiting 0.08%/cycle decay (0.2 C). These Li-S batteries are especially laudable for their performance at higher temperatures.

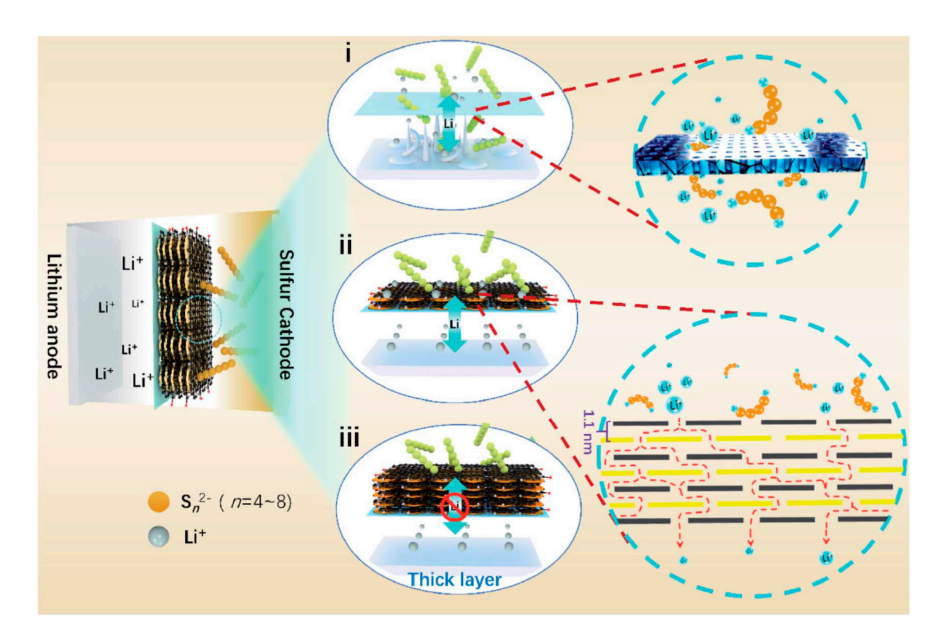


Figure 7. Schematic representation of batteries having polypropylene (PP) separator (i), ultrathin double hydroxide nanosheet/graphene oxide film-modified PP separator (ii), and thicker double hydroxide nanosheet/graphene oxide film-modified PP separator (iii). Reprinted with permission from reference [45]. Copyright 2020 Royal Society of Chemistry.

4. Cathode and Separator Materials

4.1. General Work Employing Graphene and Carbon Cathode Materials

Much of the work on Li-S batteries has focused on cathode materials or separators to provide a cathode interface [1,2,4–7], and most of those studies have employed carbon-based materials as a conductive material, physical support, or both. When lithium polysulfide (LPS) and a carbon nanofiber (CNF) composite layer are combined as a cathode and the surface is terminated with a Mo nanotube/carbon nanotube (CNT) thin film, for example, effective regulation of the electrochemical redox reactions can be attained (Figure 8) [46]. This is mediated by the Mo centers, which can immobilize the lithium polysulfide species and attenuating self-discharge activity, which is only 3% after 72 h of rest. The cell so constituted displays a high active sulfur utilization of 1401 mAh g⁻¹ (0.1 C) and has only 0.06% decay/cycle over the first 500 cycles operating at 1 C. When the cathode loading is rather high 7.64 mg cm⁻² and the cell is operated for 100 cycles, a high reversible areal capacity (4.75 mAh cm⁻²) is retained upon operation at 0.2 C. The nanoscale design of this material emphasizes what can be accomplished when adsorption sites are positioned in close proximity to both cathode material and conductive layers to effectively regulate electrochemical reaction and diffusion processes. The very small amount of Mo needed is also a plus for cost, disposal and sustainability.

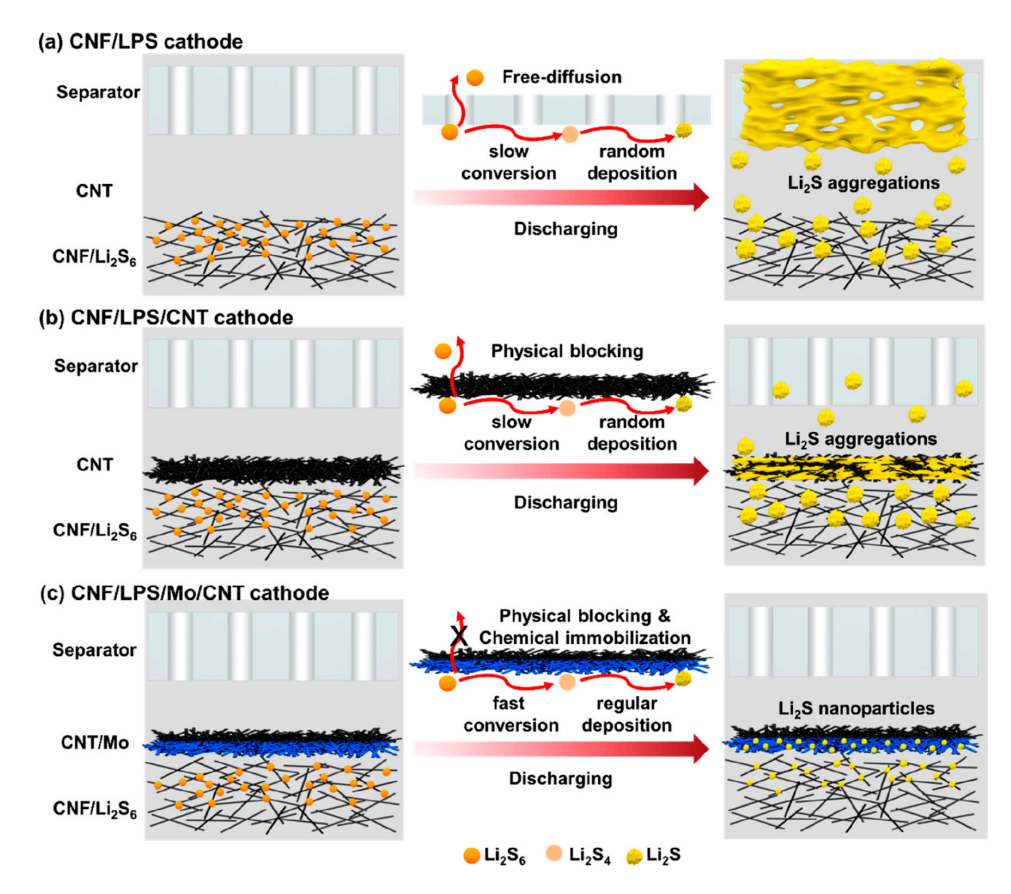


Figure 8. Schematic showing electrochemical behavior or electrodes comprising carbon nanofiber/lithium polysulfide (CNF/LPS) (a), CNF/LPS/carbon nanotube (CNT) (b) and CNF/LPS/Mo/CNT (c), the latter of which prevents free diffusion of LPS and catalyzes their conversion to lithium sulfide. Reprinted with permission from reference [46]. Copyright 2020 American Chemical Society.

Sheets comprising a few layers of graphene can also be conveniently fabricated onto carbon nanofibers to give materials appropriate to serve the dual roles of cathode scaffold and interlayer between the cathode and separator [89]. This configuration of materials led to a Li-S battery with

improved charge-discharge capacity and stability. After 100 cycles (0.5 C), a capacity of 820 mAhg⁻¹ was observed, while a capacity of 640 mAh g $^{-1}$ was still observed even after 500 cycles.

A Li-S battery has also been achieved in which a Li₂S₆ catholyte is hosted by a carboxyl-modified graphene oxide sponge having the highest specific pore volume reported to date (6.4 cm³ g⁻¹) [47]. The highly porous structure of this material successfully sequesters lithium polysulfides while displaying high electron and electrolyte transportation with commensurately improved charge storage capacity. A discharge capacity of 1607 mAh g⁻¹ (0.1 C) and areal capacity of 3.53 mAh cm⁻² were observed. Importantly, a high sulfur loading (6.6 mg cm⁻²) can be used and the devices still achieve nearly 80% active material utilization (0.1 C). After 200 cycles (1 C), a capacity fading rate of 0.065% per cycle was observed. This study especially emphasizes that the physical form taken by the material can be just as important as the chemical identity of the material used. More studies of this nature are needed to evaluate how different surface areas, porosities, etc. influence device performance of materials otherwise comprising the same molecular elements.

A sulfur host that is imbued with Lewis acidic sites to serve as potential trapping sites for polysulfides is another cathode material that is actively pursued. One study, for example, employed as the cathode support what the authors described as a "necklace-like structure" comprising interwoven carbon-nanotubes and Prussian blue ($[Fe(CN)_6]^{3-}$) nanocrystals [48]. This setup relied on the carbon nanotube array to provide conductivity and ion/electron channels, while the Prussian blue provided the necessary Lewis acidic sites to interact with polysulfides. Li-S batteries using the Prussian blue/carbon nanotube-supported cathode exhibit initial capacities of 1200 to 1457 mAh g⁻¹. Capacity retention of up to 74% (0.2 C) after 200 cycles and 61% (0.5 C) after 500 cycles were obtained. Some dependence on the amount of Prussian blue was observed, with more of the Lewis basic sites leading to better performance in general, but if Prussian blue is used alone without the carbon nanotubes, the initial capacity is only around 500 mAh g⁻¹ due to the low conductivity of Prussian blue.

Another study employing iron salts showed that Fe_2O_3 nanoparticles that are anchored in multi-walled carbon nanotubes (MWCNTs) were effective cathode components of Li-S batteries (Figure 9) [49]. Rates as high as 340 mAh g⁻¹ at 7 C-rate were achievable and stability over at least 500 cycles was demonstrated (over 545 mAh g⁻¹, at 1 C-rate). The authors attributed the impressive performance of these batteries to the ability of the Fe_2O_3 nanoparticle nodes to attenuate aggregation and dimensional swelling or to MWCNTs adsorbing polysulfides during operation, thus mitigating the shuttling issue.

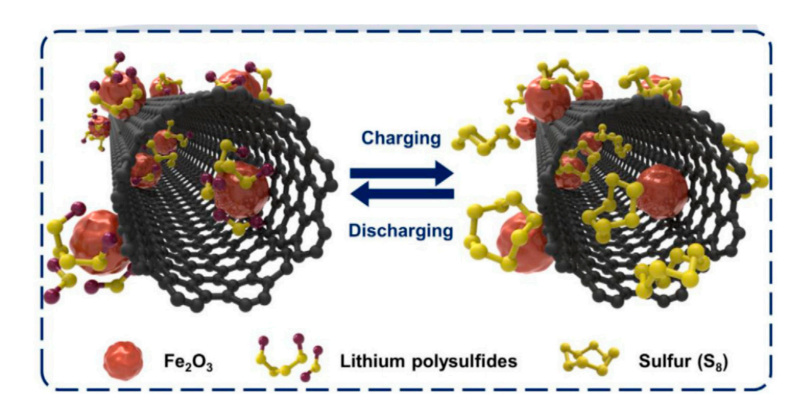


Figure 9. Schematic Demonstrating the interaction of iron oxide particles with sulfur and polysulfides during charging and discharging processes. Reprinted with permission from reference [49]. Copyright 2020 Elsevier.

Nanoparticles in graphene have also attracted significant attention. When spray-drying fabrication methods are used to combine MoS_2 nanotubes with n-doped graphene sheets, facile formation of a three-dimensional porous material was accomplished [50]. This architecture was hypothesized to facilitate conductivity due to the high surface area and the ability of electrolyte to pervade the hollow

tubes in the structure. Indeed, high reversible capacity of 1219 mAh $\rm g^{-1}$ was observed even after 200 cycles at 0.2 C. The low long-term cycling capacity decay of 0.039% per cycle over 500 cycles at 1 C and improvements in rate were also attributed to the benefits endowed by the architecture.

Although tremendous effort has been put into developing cathode materials and in devising separator layers, comparably less effort has been extended into devising porous interlayers to be placed between the cathode and the separator. This is another approach to minimize shuttle effects. In one effort in this vein, a porous interlayer was rapidly fabricated of carbon microfibers using centrifugal spinning [51]. A remarkable impact on the cell resistance was observed as a result of the interlayer. Without the interlayer, the cell had a resistance of 55 ohm, whereas the analogous cell with the interlayer had a much lower resistance of 25 ohm. When this interlayer is used, the device exhibits a high 1485 mAh $\rm g^{-1}$ initial discharge capacity. When operated over 200 cycles (0.2 C), a capacity of 615 mAh $\rm g^{-1}$. When operated at 1 C, the cell had improved performance from 250 mAh $\rm g^{-1}$ (without the interlayer) to 600 mAh $\rm g^{-1}$ with the interlayer. On the basis of these data, an important area of future work may be to evaluate Li-S batteries comprising the most successful cathodic materials and separators with the addition of such interlayers.

4.2. Heteroatom-Doped Carbon and P-Block Element Materials

One way to tune the affinity of carbon for polysulfides is to dope the carbon with heteroatoms [90]. If appropriate doping levels using a particular heteroatom is accomplished, the polysulfides can be held in close proximity to the conducting carbon near the cathode in a manner similar to that provided by Co or Mo sites, for example. Using heteroatoms instead of metals is often more affordable and more environmentally favorable as well. A recent effort to use heteroatoms employed nitrogen-doped carbon (NC) or phosphorus and nitrogen co-doped carbon (NPC) at carefully selected ratios [52]. One aim of the study, supported by calculations, was to determine the extent to which the doped materials could adsorb polysulfides (Figure 10). On the basis of simulations, a carbon nanotube aerogel was prepared using glucosamine as the nitrogen source and elemental phosphorus directly during carbonization. The cell incorporating this layer with a sulfur loading of 3.5 mg cm $^{-2}$ exhibited an initial specific capacity of 900 mAh g $^{-1}$. After 450 cycles (0.2 C), a capacity decay of 0.16%/cycle was observed. An interesting follow-up to this study would be to screen other N/P ratios experimentally to assess whether calculations and simulations are effectively predictive in these cases.

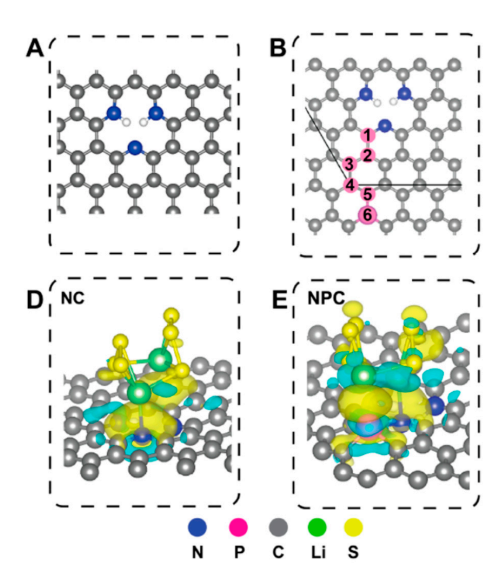


Figure 10. Schematic demonstrating the structure of NC (**A**), six types of potential P-doping sites in nitrogen co-doped carbon (NPC) (**B**), and adsorption of lithium polysulfide species (**D**,**E**) to these surfaces. Reprinted with permission from reference [52]. Copyright 2020 American Chemical Society.

Another effort employed hollow spheres comprising N-doped carbon having SnS_2 nanoparticles on their exteriors [53]. The hollow carbon spheres on their own exhibit high conductivity, and the hypothesis was that this conductivity, coupled with the high specific surface area could serve as an effective host for sulfur. A high sulfur loading of about 3 mg cm $^{-2}$ was indeed accomplished in the cathode. The purpose of the SnS_2 nanoparticles was to absorb polysulfides and facilitate the deposition of Li_2S . This cathodic material was effective in devices with a 1344 mAh g $^{-1}$ discharge capacity (0.2 C), and at 0.5 C they demonstrated reasonable stability for at least 200 cycles.

Another example of carefully-designed nanoarchitecture is illustrated by the use of hollow nanostructures, wherein pores/transport channels and strategically-positioned catalytic sites within the structure can endow enhanced transport and activity [54]. A double-shelled hollow polyhedron comprising nitrogen-doped carbon nanodots, for example, can contain cobalt nanoparticles to give such an assembly (abbreviated as Co-NC@Co₉S₈/NPC) built within the framework provided by ZIM-67 (Figure 11). The purpose of the cobalt is again to facilitate redox reaction while adsorbing polysulfides. The double-shell configuration holds materials in a confined space as a nanoreactor which cleverly suppresses the shuttle effect while enhancing ion/electron transport. Over an impressive 2000 cycles, the capacity decays only 0.011% per cycle (2 C). After 500 with a high sulfur loading (4.5 mg cm⁻²) the cell still operated very efficiently, validating the benefit of the nanoconfinement approach. Several other studies on hollow structures to serve as nanoreactors and to control volume changes have also been noted recently, as discussed below.

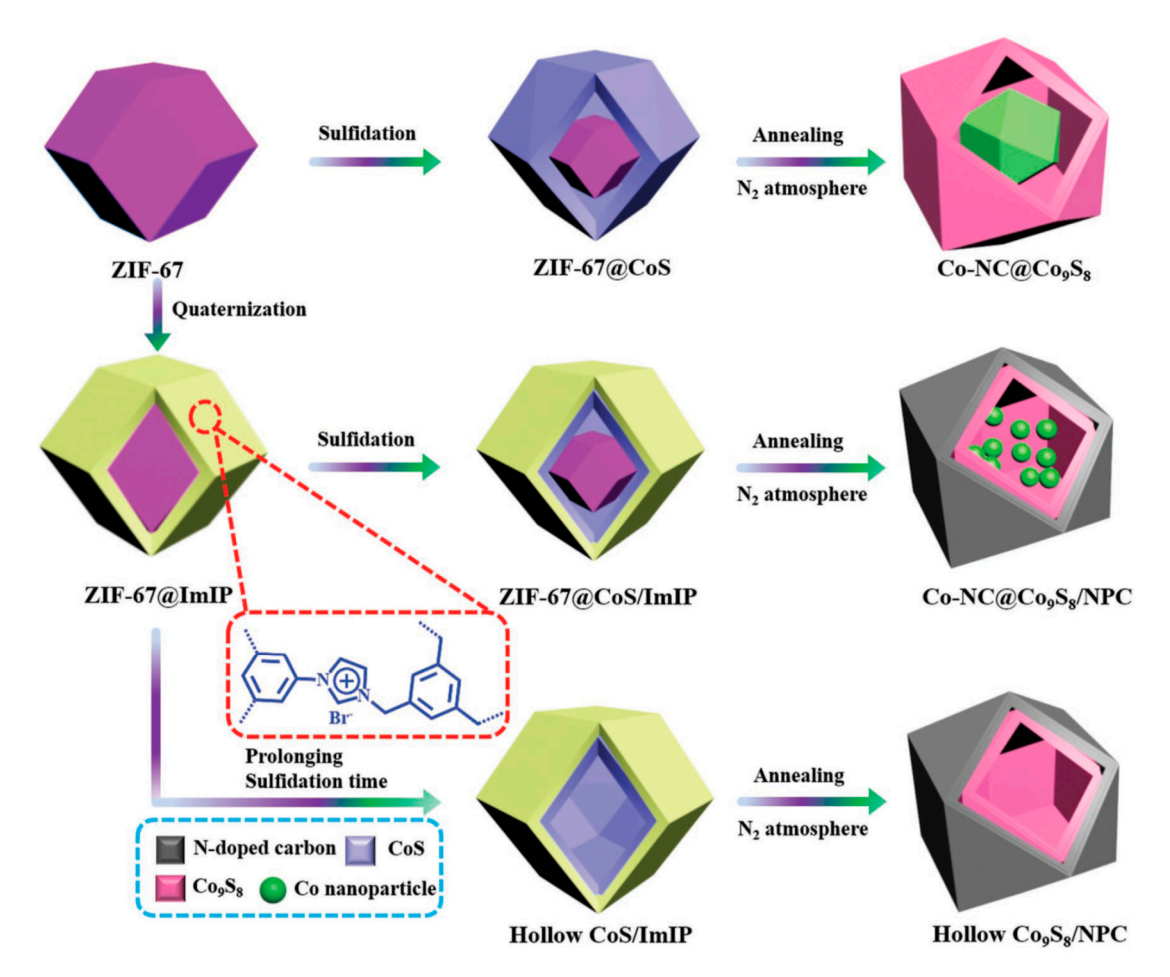


Figure 11. Schematic demonstrating the assembly of double-shelled hollow polyhedron comprising nitrogen-doped carbon nanodots. Reprinted with permission from reference [54]. Copyright 2020 John Wiley and Sons.

Despite the benefits afforded by hollow pore-containing systems, there is some drawback to having such a high sulfur loading due to a lack of ability for all the sulfur to interact with electrolyte. In a recent study, researchers have addressed this by installing rib-like supports within their hollow carbon structure (Figure 12) [55]. Resultant radially-aligned systems have a very well-defined set of pores, facilitating the efficient infusion of sulfur into the channels. To further enhance the propensity of this system to block polysulfide species, nitrogen-doped carbon nanospheres were also employed in such construct. After 1000 cycles Michelle comprising this electrode material displayed a capacity loss of 0.044% per cycle, somewhat higher than in the ZIM-67 materials discussed above.

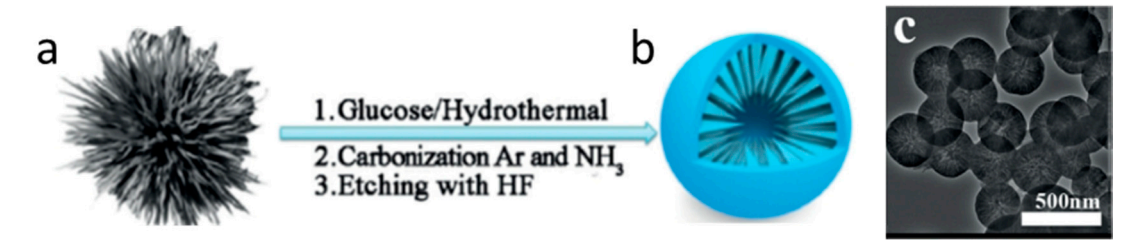


Figure 12. Use of silica particles (**a**) as a scaffold for assembly of hallow carbon nanospheres (**b**) having silica rib-like fine structure on the interior, as demonstrated in an SEM image (**c**). Reprinted with permission from reference [55]. Copyright 2020 John Wiley and Sons.

Another study sought to explore the impact of combining nitrogen-doped carbon nanotubes in tandem with metallic cobalt nanoparticles [56]. As has been discussed in earlier examples, either heteroatom-doped carbon or metal nanoparticles alone can help adsorb and confine polysulfides near the conducting support. The question to be addressed in this study is whether there is a benefit or synergy between the two materials for overall device performance. The Li-S battery employing this dual-component material, indeed, has excellent cycle stability: after 500 cycles, a capacity decay of just 0.08% was observed (1 C). At higher current density (5 C), capacity of 530 mAh $\rm g^{-1}$ was still possible, representative of the quite good performance of these cells even with a reasonably high sulfur loading of 4 mg cm⁻². The capacity decay of these combined Co/N-doped carbon systems outperform the aforementioned cells that employed N- and P-doped carbon, the former having half the rate of capacity decay compared to the latter (0.08%/cycle versus 0.16%/cycle).

Higher capacity over more cycles can be accomplished, albeit at the cost of more involved cathode material fabrication. For example, a B,N co-doped carbon nanotube material with additive Co nanoparticles was employed as a sulfur host for a Li-S battery cathode material [57]. The assembly so composed provided high sulfur loading while also lowering dimensional expansion during operation and suppress the shuttle effect. This advantageous combination thus facilitates a good capacity of 1160 mAh $\rm g^{-1}$ over not less than 200 cycles (0.1 C) and 1008 mAh $\rm g^{-1}$ after 400 cycles (1.0 C), corresponding to a loss of only 0.038%/cycle.

One hurdle to commercial applications of doped carbon is the cost of their manufacture. For this reason, recent efforts have focused on devising an affordable synthesis that might allow for scalability. In one such effort, a nitrogen-doped carbon material was prepared from commercial carbon black and melamine by simple thermolysis [91]. This process was demonstrated on 100 g batches using various carbon: melamine ratios and pyrolysis temperatures. Cells having sulfur-carbon cathodes that incorporated N-doped carbon so-prepared exhibited rather moderate performance, but the need for scalability to bring high-performance Li-S batteries from academic to commercial utility is an important issue that requires extensive additional study.

Another heteroatom combination that has been tested is phosphorous/oxygen co-doped into mesoporous carbon bowls (Figure 13), putatively as P_2O_5 [58]. One stated rationale for using the bowl shape is the high surface tension that can be induced in the structure, resulting in its enhanced reactivity. This material endows its composite cell with an initial capacity of 897 mAh g^{-1} (1 C). After 800 cycles, however, only 489 mAh g^{-1} of this is retained, corresponding to a capacity loss of

0.06%/cycle. Cells with this electrode do support a high areal capacity of 5.5 mAh cm $^{-2}$ at a sulfur loading of 5.02 mg cm $^{-2}$, however.

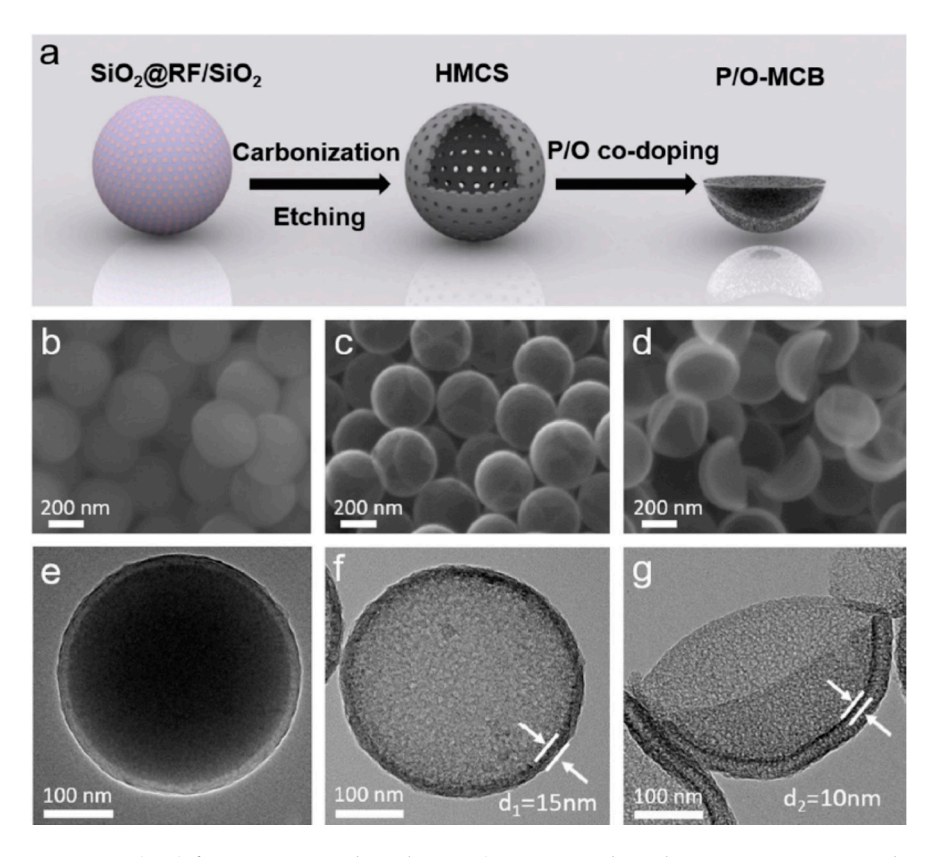


Figure 13. Process (**a**–**c**) for preparing phosphorous/oxygen co-doped into mesoporous carbon bowls (**d**,**g**) from initially-formed spheres (**b**,**c**,**e**,**f**). Reprinted from reference [58], © 2020 used with permission from Elsevier.

An interesting approach that is rather new in this field is to use defect engineering to endow their composite materials with advantageous properties. In one example, anion-deficient antimony selenide (Sb_2Se_{3-x}) is employed as a polysulfide barrier [59]. As the material is anion deficient, it provides natural docking sites for the polysulfide anions. The high affinity in turn promotes fast kinetics sulfur electrochemical conversion. Superior Li-S battery performance results, as even after over 500 cycles a capacity fading rate of only 0.027%/cycle (1.0 C) wan noted with a high areal capacity of 7.46 mAh cm⁻². Defect engineering thus holds great promise for tuning Li-S performance, and a wide range of main group sulfides may be envisioned for utility in this regard.

A simplified approach to cathode assembly involving simple co-melting of sulfur and selenium, its heavier main group congener, has also offered some intriguing preliminary results [60]. This chalcogen alloy was fabricated into a composite with reduced graphene oxide to serve as a readily-produced cathode (areal loading of electroactive material attained 6.5 mg/cm 2). Li-S batteries encompassing this cathode showed modest capacity of 800 mAh g $^{-1}$ over at least 100 cycles.

Inorganic separators, such as those comprising affordable anodized aluminum oxide membranes [61] can be a cost-effective alternative to organics that, in addition to being cheaper, also afford improvements in terms of being nonflammable, an important consideration for Li ion battery safety. Initial studies on anodized aluminum oxide membranes are quite promising, as the composite batteries display high lithium ion transport, low areal specific resistance, and low overpotential of Li deposition/stripping. Li-S batteries employing the separator had a degradation rate of 0.105%/cycle after 480 cycles (2 C).

One rather novel approach to growing a cathode material was to grow carbon fibers from the vapor phase to penetrate sulfur crystals [92]. A reasonable areal mass loading and capacity (3.4–4.4 mAh cm $^{-2}$) were achieved with this cathode. Between 93–97% of capacity is retained at low current densities (0.2–0.5 C) Concerning the stability of the capacity, 90% of the initial 920 mAh g $^{-1}$ capacity is retained after 200 cycles (0.1 C), with a reported coulombic efficiency of 100%.

4.3. Less Common Allotropic Forms of Carbon and Sulfur

Although carbon nanotubes and graphene elements play a central role in Li-S and many other emerging electrochemical technologies, more recently engineered allotropes of carbon, such as graphynes, may well prove to be important elements in such technologies as well. An interesting example is the recent exploration of graphdiyne nanosheets imbued on a polypropylene membrane (GDY-PP, Figure 14) as a separator [62]. This design has merit in improving the adsorption of polysulfide species on the basis of the increased electronegativity of sp-hybridized carbon atoms in the diyne units. These sp-hybridized carbon atoms are not present in typical graphene or carbon nanotubes, which comprise exclusively sp^2 -hybridized carbon atoms. This chemical intuition was born out in the performance of the cell, which displayed a high initial capacity (1262 mAh g^{-1} , 0.1 C) and after 500 cycles still exhibited a capacity of 412 mAh g^{-1} at 1 C. As illustrated by the performance of this initial cell, utilizing additional graphyne and related emerging carbon allotropes should certainly be pursued as an avenue to find the optimal separator layers for Li-S batteries.

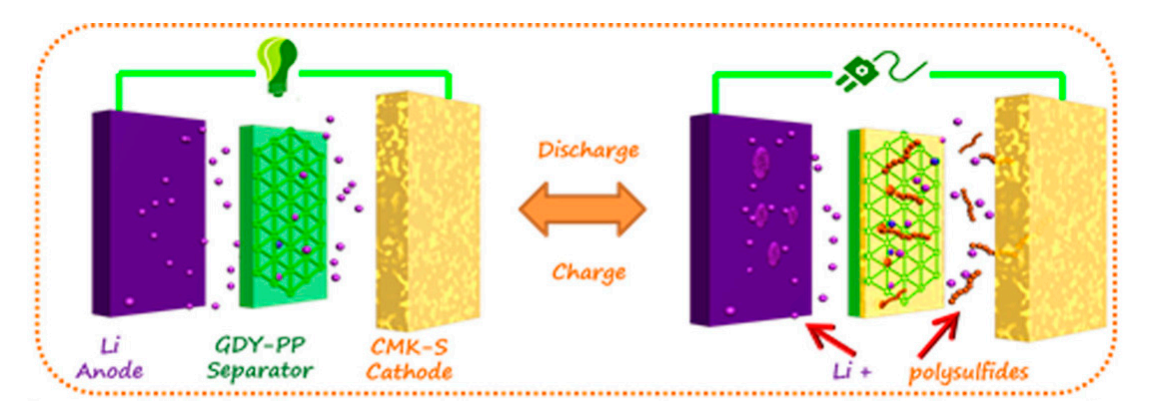


Figure 14. Schematic illustration of the role of the separator comprising graphdiyne nanosheets imbued on a polypropylene membrane (GDY-PP). Reprinted from reference [62], © 2020 used with permission from the American Chemical Society.

Just as new allotropes of carbon are being developed for use in Li-S batteries, new forms of sulfur are also prime targets for evaluation. At standard temperature and pressure (STP), sulfur's most prevalent allotrope is as an S_8 ring in a solid, orthorhombic crystalline state. In 2019, it was reported that a liquid form of sulfur can be generated in an electrochemical cell in a supercooled state well below the melting point of orthorhombic sulfur [93]. The researchers who made this remarkable discovery quickly recognized that such a new form of sulfur should be evaluated in Li-S battery contexts [94]. In the initial study in this vein, it was revealed that very different areal capacities are achieved with the supercooled liquid sulfur versus the typical solid sulfur, but most of the study focused on understanding the morphology and phase changes in space during operation of the cell, so a full picture of how supercooled liquid sulfur might perform in Li-S batteries of various configurations remains to be elucidated. Much more work will need to be done to evaluate the performance of this new form of sulfur and other forms of sulfur that may be attainable.

An emerging technique for the synthesis of high sulfur-content materials is by inverse vulcanization [63]. Since these materials can often stabilize oligomeric or polymeric forms of sulfur that may have different electrochemical performance than the usual S₈ allotrope, materials made by inverse vulcanization should be carefully and thoroughly pursued as an element of lithium sulfur batteries.

The utility of high sulfur-content materials prepared via inverse vulcanization for Li-S batteries has been so hotly pursued recently that the area was recently reviewed [95]. Since that review, however, other reports have emerged. One example [96] employs poly(sulfur-co-1-vinyl-3-allylimidazolium bromide) made by inverse vulcanization of S_8 with an ionic polymer. The dual role of this material as cathode and polysulfide suppression material was demonstrated and supported by DFT calculations as well. The cell employing this cathode retained over 90% of its initial capacity even after 900 cycles.

4.4. Semiconducting, Hyperbranched and Inert Polymer Supports and Separators

An approach to preparing flexible batteries [97,98] is to employ organic semiconducting polymers such as polyaniline (PANI, Figure 15) as a component of the conducting layers [64]. When MnO_2 nanoparticles are embedded in PANI, a porous network forms that can be used as a scaffold for the sulfur cathode. Scaffolding reduces volume changes associated with unsupported sulfur cathodes. A synergistic result of the channels provided by the scaffolding material is that the channels improve transport of ions and carrier species through the electrode as well. The chemical composition of the scaffold to include a semiconducting polymer also facilitates conversion of polysulfide species to thiosulfates. This in-cathode chemical reactivity should significantly attenuate the shuttle effect. The initial study on a Li-S battery employing this scaffolded cathode displayed stable capacity as high as 1195 mAh g^{-1} at 0.5 C even after 100 cycles. A discharge capacity of 640 mAh g^{-1} at 2 C was achievable even after 500 cycles with this configuration.

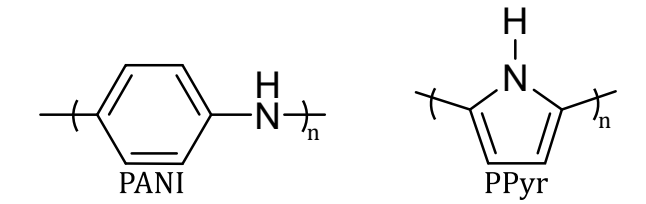


Figure 15. Chemical structures of polyaniline (PANI) and polypyrrole (PPyr).

Another effort to combine the conductivity of an organic semiconducting polymer with a metal oxide employed polypyrrole (PPyr, Figure 15) and tin oxide nanoparticles [65]. The use of polypyrrole indeed improved the conductivity of the cathode and effectively hindered polysulfide diffusion due to the polarity of the backbone structure. The tin oxide particles also served to trap polysulfides through covalent bond formation. A cell fabricated to include \sim 65 wt % sulfur in the cathode was operated for 500 cycles (1 C) and exhibited a capacity loss of only 0.05%/cycle. At higher current density (5 C) 383.7 mAh/g at 5 C was attainable with coulombic exceeding 90%.

Polypyrrole can also be incorporated by in situ polymerization within a mesoporous silica framework having NiO nanoparticles dispersed in it [66]. This mesoporous material effectively provides physical trapping of polysulfide species as they migrate through it as well as formation of chemical bonds to the polysulfide species. A high capacity stability is affected by this material, and even after 300 cycles the capacity holds at \geq 700 mAh g^{-1} .

Semiconducting poly(N-methylpyrrole) can also be used in conjunction with S@reduced graphene oxide [99]. A recent application of this composite was in conjunction with a polymer gel electrolyte fabricated by combining silica nanoparticles with lithium imide and poly(methyl methacrylate). The intimate contact between the polypyrrole derivative and the gel electrolyte provides outstanding Li ions exchange between layers and the Li ion diffusion coefficient can be as high as $10^{-6}~\rm cm^2~s^{-1}$. The high lithium ion conductivity is accompanied by commensurately low polysulfide species permittivity through the material. This is manifest in device performance, wherein the capacity retention after 500 cycles is 3-fold higher when the gel electrolyte is used compared to traditional organic electrolytes. The use of gel electrolytes, fire-retardant electrolytes and solid-state electrolytes have all shown great promise in solving some safety issues and alleviating the shuttle effect in recent work in the field.

Earlier studies suggested that hyperbranched polymers, such as those prepared by inverse vulcanization [63] may also prove effective as cathode support materials in Li-S batteries [100]. Recently, a polymer-encapsulated sulfur cathode strategy [67] thus used HPEIGA, a readily-synthesized hyperbranched material prepared from polyethyleneimine and glutaraldehyde. The hyperbranched material serves the dual role of having low permeability to polysulfide species due to the pore size, but also as an effective chemical absorbent of polysulfides through their interaction with nitrogen atoms in the structure. This hyperbranched polymer thus had a shuttling current that was 81% lower than when a typical carbon nanotube-sulfur cathode is used. The result was a battery that retains 74% of its capacity at 2 C even after 600 cycles.

Polypropylene is one of the most prevalent polymers in use primarily because of its chemical inertness. This property was recently exploited in using a functionalized polypropylene as a scaffold for a polysulfide-blocking separator layer [68]. The polypropylene membrane was first modified with cubes comprising cobalt phosphide on carbon (Figure 16) that were then embedded into polypropylene as a separator. The cobalt phosphide material proved effective in capturing polysulfides and in catalyzing conversion of soluble intermediates with good kinetics. The Li-S battery comprising this effective separator layer showed an initial capacity of 938 mAh $\rm g^{-1}$ and this capacity decayed by only 0.08% per cycle even after 500 cycles (1 C). Even with a high sulfur loading (3.2 mg cm⁻²), the cell displayed a reversible capacity of 601.3 mAh $\rm g^{-1}$ even after 100 cycles (0.5 C). As this work exemplifies, the use of more inert membrane materials is an important strategy. Most of the separator layers that employ a polymer have used ionic or very polar units that are susceptible to reaction over time. Creative strategies to employ modified nonpolar, inert polymer backbones should be an area of increased research to achieve the potential of Li-S batteries for long term operational life.

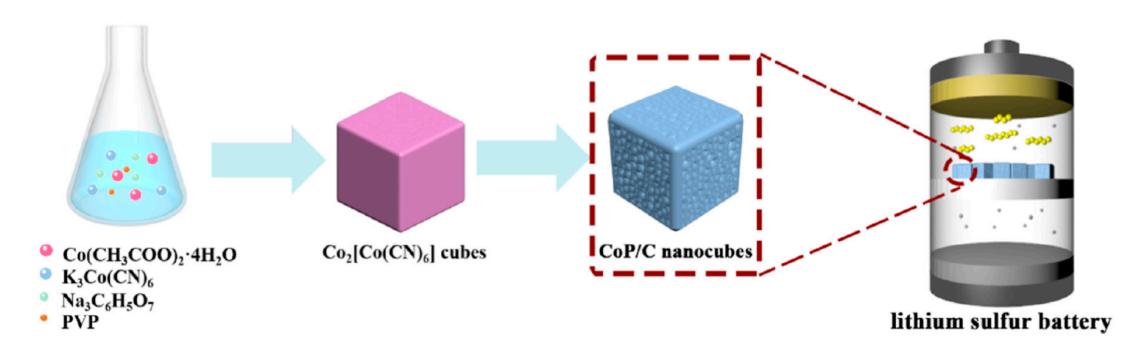


Figure 16. Schematic illustration of use of cobalt phosphide (CoP)-modified carbon cubes in a separator layer. Reprinted from reference [68], © 2020 used with permission from the American Chemical Society.

4.5. Biopolymers in Li-S Batteries

Despite the intense interest in developing strategies to suppress the shuttle effect, there is still work to be done to understand the structure–property relationship relating the structural features of molecules comprising interlayers and separators to the ability to sequester, react, or absorb polysulfides. For many synthetic polymers and well-defined nanomaterials these concepts are well studied, yet the issues are more complex when natural biopolymers are used. Biopolymers are important targets for sustainability, so understanding their influence on device performance in spite of their compositional diversity is an important problem. One study aimed at addressing this issue used natural gelatin and denatured zein proteins to fabricate nanocomposite interlayers with carbon nanofibers [69]. This study illuminated a dependence of device performance on protein sidechain lengths (Figure 17). Gelatin, which has shorter sidechains on average than does the zein protein, shows significantly stronger adsorption of polysulfides. Consequently, the gelatin-carbon nanofiber interlayers facilitate high sulfur loading at the cathode (9.4 mg cm⁻²). A high areal capacity of 8.2 mAh cm⁻² (0.1 C) was maintained over 100 cycles. Given these results, a systematic study on sidechain lengths and

composition employing polar proteins like gelatin could be an important next step to fully delineating the structure–performance understanding.

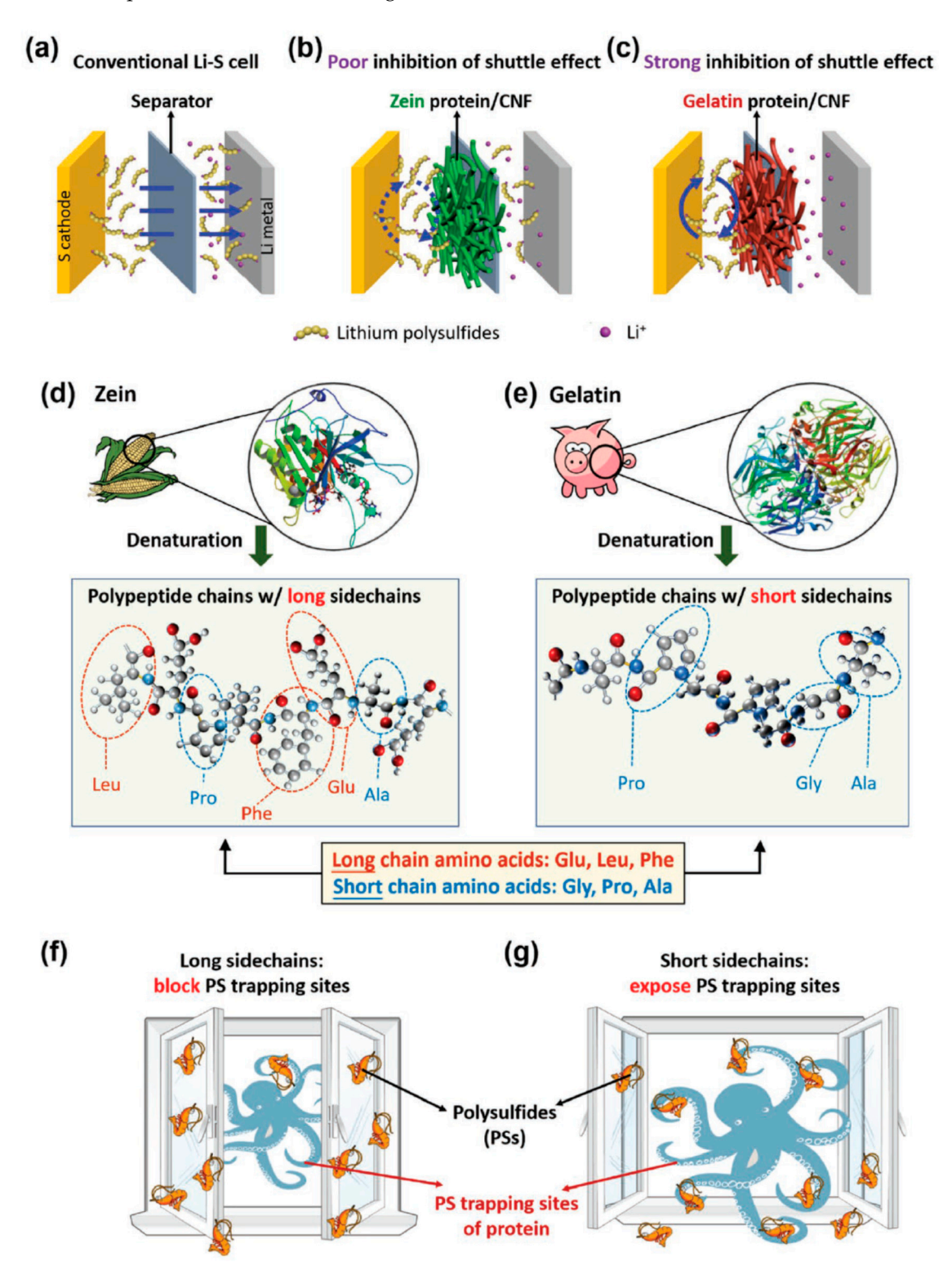


Figure 17. Demonstration of the source, structure, and utility in Li-S batteries for biopolymers. Reprinted with permission from reference [69]. Copyright 2020 John Wiley and Sons. Whereas conventional Li-S batteries (a) and those employing zein (b) cannot effectively limit the shuttle effect, gelatin provides superior inhibition (c). This effect is attributed to the long sidechains in zein (d,f) compared to the short sidechains in gelatin (e,g).

Another effort on interlayer fabrication employed carbon nanofibers, in conjunction with konjac glucomannan (KGM, Figure 18), a naturally-occurring polysaccharide that comes from the root of the konjac plant [101]. The polysaccharide-carbon nanofiber motif was made into an interwoven mat-like thin layer with carbon nanofibers (CNFs) with the hopes that it would effectively trap polysulfides. This was hypothesized to be a more effective trapping layer because the polysaccharide is highly polar and, therefore, should more strongly interact with polysulfides compared to the carbon nanofiber mats alone [70]. From a sustainability standpoint, this is an attractive approach because not only are the raw materials a biopolymer and carbon nanofibers (which can be made from biomass), but the fabrication is also carried out in green solvents such as ethanol and water. The aforementioned high chemisorption power of the polysaccharide was credited with attenuating shuttle effects, resulting in high performance of the Li-S batteries using this interlayer. A quite reversible capacity of 1286 mAh g⁻¹ (0.2 C) was observed initially, and a capacity retention of 84% is observed even after 400 cycles at 1 C.

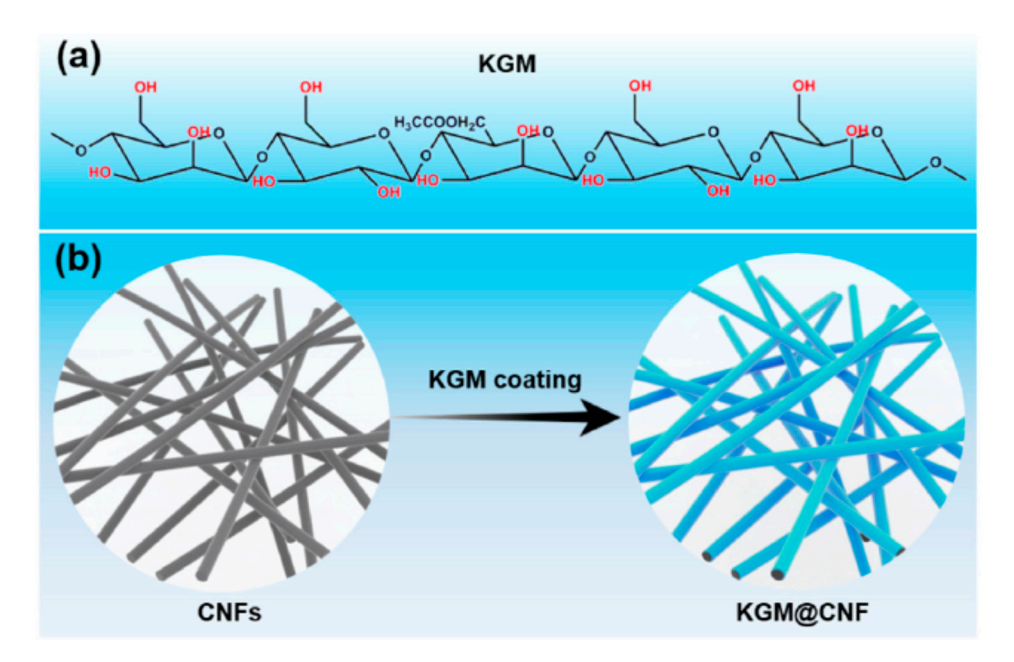


Figure 18. Structure of konjac glucomannan (KGM, (a)) and schematic for how it is made into a mat of KGM-coated fibers to be used in a Li-S battery (b). Reprinted from reference [101], © 2020 used with permission from Elsevier.

Rather than modify the cathode itself, some researchers have explored the effect of various separator layer. A novel strategy in this area was to add a sodium alginate derivative affinity laminated chromatography membrane into the system [71]. This type of membrane is traditionally used in selective protein adsorption, an application space in which affinity relies at least in part on the variation in surface charge on the proteins. This made them good candidates for selective adsorption (or blocking) of polysulfides. With added layers of this nature, a high initial capacity of 1492 mAh $\rm g^{-1}$ was achieved at 0.1 C, with capacity retention of 76% at 0.2 C after 200 cycles. The researchers also accomplished high-loading electrodes with initial capacity of 1302 mAh $\rm g^{-1}$ at 0.05 C and capacity retention of 95.2% at 0.1 C after 40 cycles.

Another type of separator that proved effective for trapping of polysulfides was prepared by the carbonization of urea and amylose (a polysaccharide starch) in the presence of nickel chloride [72]. This separator maintained conductivity of Li⁺ ions and electrons while providing significantly improved reaction kinetics. The Li-S batteries comprising this separator had an exceptionally low decay rate (0.043%/cycle, 4 C) with a high cathode loading (7 mg cm⁻²) and low electrolyte content (7.8 μ L mg⁻¹). Batteries so configured provided a discharge capacity of 714 mAh g⁻¹ even after 100 cycles. The clever

design of this system provides insight into future systems wherein catalytic nanoparticles can be combined with more traditional layer architectures.

As the synopses of the last few studies reveal, polar biopolymers like gelatin and polysaccharides have good barrier properties for suppressing the shuttle effect. The variable and complex composition of biopolymers have been cited as a drawback of trying to use them on a large scale, however, leading some researchers to evaluate highly polar synthetic polymers. In one such study, an interesting approach using a polymeric zwitterion was employed as an interlayer [73]. The authors hypothesized that the cationic sites would exhibit good sulfophilicity while the anionic polymer sites would exhibit good lithiophilicity. This dual associative driving force would be expected to support good ion transfer. The zwitterionic polymer interlayer proved highly successful. Indeed, whereas most of the studies described herein test devised over 100 to 500 cycles, the Li-S batteries having the zwitterion polymer interlayer could be operated for 1000 cycles, over which a loss of capacity of only 0.012% per cycle was observed, and a high areal capacity retention of 5.3 mAh cm⁻² was noted even after 300 cycles.

With an eye towards more sustainably-sourced battery material, some researchers are targeting the abundant lignocellulosic biomass waste as a precursor rather than using isolated biopolymers. This approach was recently reviewed [38]. In one investigation into biomass that was reported since the latest review, corncob material was reacted with sulfur to form a composite material that was tested as a cathode in Li-S batteries [74]. These batteries exhibit good initial performance but poor stability with recursive cycling. To assess the extent to which oxygen content influenced the performance of these green batteries, several additional carbon matrices were screened wherein the surface areas were held essentially constant but oxidation was varied by reaction with nitric acid followed by reduction. The oxygen content was thus varied from 4.4 wt % to 20.4. Through this study the authors were able to unveil batteries having an initial discharge of up to 1504 mAh g^{-1} that can be maintained to 799 mAh g^{-1} after 200 cycles (0.3 C) for the lowest-oxygen carbon matrix.

4.6. Metal-Organic Frameworks (MOFs) and Other Open-Pore Scaffolds

In another demonstration, TiO_2 is used as part of a metal organic framework prepared by the reaction of TiO_2 and terephthalic acid [102]. In this case the authors tested the influence of just adding terephthalic acid or just adding the titanium dioxide. The metal organic framework composed of the two components together outperformed either of the individual components by a wide margin. Like the other men metalorganic framework materials described here in this systems suppress dendrite growth and improve cell cycling lifetime.

An emerging trend towards more atomic-level control is manifest in a series of studies wherein MOFs are employed as components of Li-S batteries [75]. One such example employs sulfurized polyacrylonitrile in conjunction with carbon nanotubes and conductive CoS_2 as an especially well-performing cathode material. Fibers supporting the cathode were grown in situ to create a zeolitic imidazolate framework (ZIF-67, Figure 11) on polyaniline/carbon nanotubes prior to reaction with sulfur. The main drawback of this system is its low sulfur content (~40 wt %). However, the use of an organic polymer as the primary support for this cathode material portends its utility in the flexible or wearable battery technology application space. As was the case with Ni nanoparticles described in the prior study, the CoS_2 has a beneficial effect on the kinetics of sulfur conversion and consequent downstream improvements on the areal capacity. Indeed, an initial areal capacity of 8.1 mAh cm-2 is achieved with an impressive sulfur loading of up to (5.9 mg cm⁻²) and high capacity (1322 mAh g⁻¹).

Another application of the ZIF-67 fiber material [103] was in conjunction with cobalt nanoparticles and dicyandiamides. Although a somewhat lower sulfur loading was achieved in this material (4.3 mg cm^{-2}) , a reasonable areal capacity of 3.73 mAh cm^{-2} was possible after 100 cycles (0.1 C).

A third application of the ZIF-67 framework [104] was as a component of electrospun Co, N, CNF mats to serve as $\rm Li_2S_6$ containing catholyte current collectors (Figure 19). This design established the accelerated redox kinetics for lithium polysulfides/sulfide. A high sulfur loading of 4.74 mg/cm⁻² was possible and this cell gave initial capacity of 1166 mAh g⁻¹ of which 938 mAh g⁻¹ was retained after

300 cycles (0.2 C). A cell fabricated with higher sulfur loading (7.11 mg/cm⁻²) still had a high areal capacity of 6.47 mAh cm⁻². Given the promising performance of these few ZIF-67-containing cells, more studies on this and related MOF materials will be worth pursuing in future cell design.

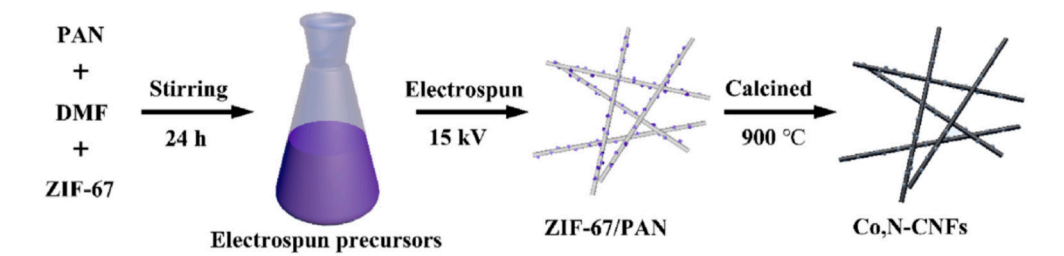


Figure 19. Electrospinning technique to prepare high surface area mats of Co,N-CNFs. Used with permission from reference [104], © 2020 used with permission from Elsevier.

Carbon nitride might be conceptualized as an extreme form of nitrogen-doped carbon. As such, carbon nitride has high conductivity, but also has the ability to sequester polysulfide species. One study to capitalize on these beneficial properties of carbon nitride is by utilizing them as components of a MOF that served as a separator layer [105]. Cells in which this separator layer are employed demonstrate a high initial capacity of 1532.1 mAh g $^{-1}$ (0.2 C). Rate capabilities of around 1000 mAh g $^{-1}$ were achieved at higher current densities (1.0 and 2.0 C). These cells display a remarkably high cycling stability even after 12,000 cycles, after which they retain 88% of their capacity (as the capacitive electrode). This carbon nitride system thus represents another viable candidate for metal free-fabrication of Li-S batteries.

When nitrogen is doped into a MOF containing dispersed cobalt catalysts, a porous material results [106]. This material can be used as a sulfur host in the cathode. The rationale for this cathode composition is again to capitalize of the polysulfide sequestration afforded by the heteroatom dopant and metal sites, but in synergy with the porosity and surface area of contact between the scaffold and the sulfur that is afforded by the MOF. The open framework structure also allows for advantageously high sulfur loading. Indeed, a Li-S battery comprising this cathode displays fast kinetics for ion and charge transport and good redox reaction kinetics for polysulfides. When operated at 1 C for 500 cycles the cell can maintain 86% of its capacity, while at higher current density (5 C), a high rate performance of 600 mAh $\rm g^{-1}$ was accomplished.

Ultrathin sheets of MOFs have proven to effectively improve the safety of Li-S batteries by homogenizing Li ion flux due to their adsorption (at the anode side of the sheets) by the oxygen atoms in the framework [107]. Cobalt likewise serves to sequester polysulfides. These features lead to composite cells that exhibit low capacity decay (0.07%/cycle) after 600 cycles. An areal capacity of 5.0 mAh cm⁻² is also achieved with high sulfur loading (7.8 mg cm⁻²) The cell can be made to be rather flexible and was even demonstrated to perform well even when bent at defined angles.

One MOF study utilized carbon cloth, graphene nanocloth, and cobalt phosphide components grown on graphene [108]. This service at cathode support for sulfur at a loading of 2 mg cm $^{-2}$. This cathode provided a very high rate capability of 930.1 mAh g $^{-1}$ (3.0 C) with only capacity loss of only 0.03%/cycle after 500 cycles (2.0 C). When higher sulfur loadings of up to 10.83 mg cm $^{-2}$ are employed, a high areal capacity of 8.81 mAh cm $^{-2}$ (0.05 C) is possible. This is quite a high sulfur loading, so such freestanding cathode scaffolds may support improved batteries as the technology is further explored.

A nitrogen-rich MOF was employed to capitalize on the polysulfide blocking ability of the polar structure and to utilize the open pore structure of the framework to facilitate trapping of sulfur in the cathode as well as to facilitate high surface area [109]. This framework structure was decorated with iron nanoparticles to serve as a catalyst to mediate the redox reactions. The combination of the open framework with the iron catalyst effectively gave good redox kinetics as well as a high sulfur utilization. A specific capacity of 1123 mAh $\rm g^{-1}$ was attained using this cathode (0.2 C), while at a

higher current density, a capacity of 605 mAh g^{-1} was attained and even over 500 cycles a low capacity loss of 0.06%/cycle was observed.

Whereas a plethora of studies employ either Mo or Co oxide nanoparticles, one study sought to harness both metals in the form of 3D, hierarchically-structured $CoMn_2O_4$ microspheres as sulfur hosts in the cathode [110]. The assembly of hollow spheres provided a scaffolding appropriate for high sulfur loading while preventing dimensional expansion during cycling. The intimate nanoscale contact of the $CoMn_2O_4$ microspheres with sulfur provided an ideal setup for catalytic conversion of polysulfides, thus alleviating the shuttle effect to great extent. The Li-S batteries employing this cathodic formulation had a high tap density of 1.73 g cm⁻³ and capacity as high as 907 mAh cm⁻³ (at 1600 mA g⁻¹).

In another study employing open pore structures, lithium sulfide was placed in a three-dimensional mesoporous carbon architecture (CMK3, Figure 20) [111]. The very large volumes of free space available in this architecture facilitate volume changes that may be necessary during cell operation as well as providing a high surface area or redox reaction. This structure successful supported a 79 wt % loading of sulfur into the material and the battery comprising this cathode material exhibit a high specific capacity of 848 mAh g^{-1} (0.1 C) or 410 mAh g^{-1} after 400 cycles at higher current density (2 C).

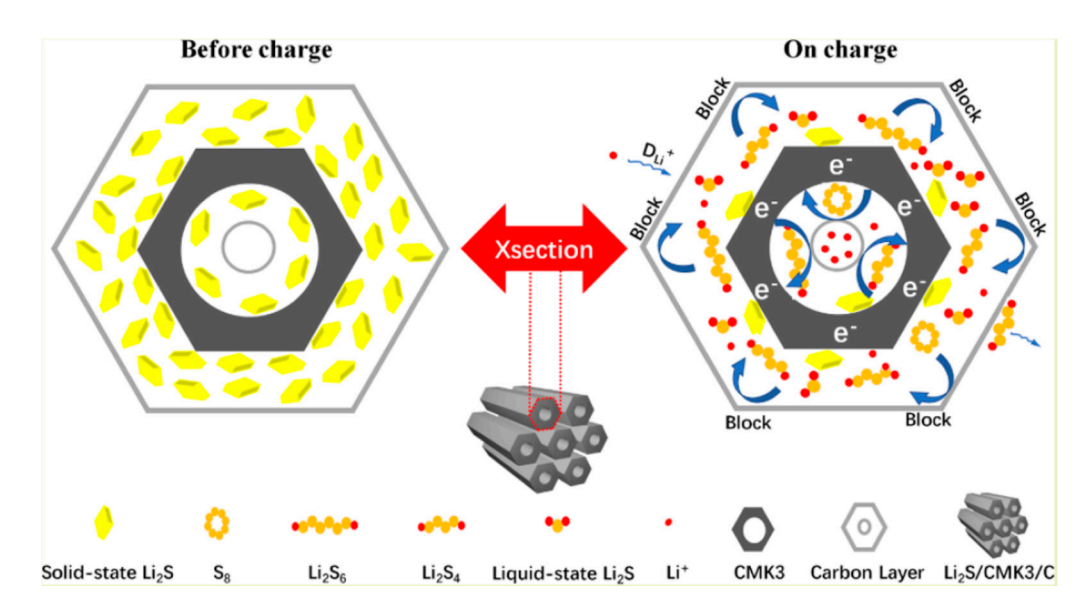


Figure 20. Schematic illustration of use of CoP-modified carbon cubes in a separator layer. Reprinted from reference [111], © 2020 used with permission from the American Chemical Society.

In another report, free volume was accomplished by using hollow spheres of titanium oxide and titanium nitride [76]. This provides a tandem system wherein the titanium oxide is expected to provide high absorptions of polysulfide species [77], whereas the titanium nitride will provide high conductivity. Cells employing this cathode as part of their design exhibit a very high initial specific capacity of 1254 mAh g^{-1} . After 500 cycles the cell displays coulombic efficiency up to 99% and a reversible capacity of as high as 533 mAh g^{-1} (0.2 C). Such a novel combination of compatible conducting and adsorbing units is a well-founded strategy that could have great utility in future studies.

4.7. Systems Employing Metal Sulfides and Phosphides

Metal sulfides have long been considered as potential components of Li-S batteries on the basis of their affinity for polysulfide species [112]. If this affinity could be coupled to beneficial reactivity to allow the polysulfides to transform to active species, for example, performance and device lifetime could be improved. Thus far, however, the slow kinetics of redox reactions at metal sulfides in these systems has been a barrier to their effectiveness. A recent study [113] sought to improve surface area and reactivity of metal sulfides, specifically $\text{Co}_3\text{S}_4/\text{MnS}$ nanotubes, by growing them on a cotton cloth

for use as a battery layer. This configuration was based on prior work suggesting that Mn dopants will improve the reactivity of Co_3S_4 sites with the target polysulfides. A battery including this metal sulfide-doped cotton cloth with a 3.2 mg/cm⁻² loading of sulfur as a cathode was prepared and it exhibited cycle performance at a charge density of 2.67 mA cm⁻² with 95% retention of initial specific capacity even after 200 cycles.

Nickel sulfide Ni_3S_2 can be fabricated into a N/S-doped reduced graphene oxide to heal the hybrid material having a large specific surface area and efficient polysulfide capture [114]. This system takes on a pleated 3D structure comprising a conductive network with specific surface area of 618 m² g⁻¹ and a pore volume of 1.73 cm³ g⁻¹, as measured by the method of Brunauer–Emmett–Teller (BET). Both of these metrics are cited as the highest among hybrid materials studied for Li-S batteries. Even after 1000 cycles at a relatively high current density (3 C), the cell only suffers capacity loss of 0.023%/cycle. Specific capacity of 6.72 mAh cm⁻² (at 0.05 C) is attainable for a sulfur loading of 5.8 mg cm⁻². This is another example in a series of studies described herein that demonstrate the emerging effort to harness tandem and hybrid materials to act in synergy for improved cell performance.

Hollow architectures have been explored as geometries to improve surface area and to control volume expansion effects in Li-S batteries [115]. One hollow architecture that has been explored comprises a combination of zinc sulfide and iron sulfide encapsulated in a nitrogen-doped carbon structure [116]. Compared to cobalt, comparatively few studies have been done utilizing zinc and iron. This particular study confirmed that the kinetics of the redox reactions and ion charge transport are both rather good in this system. A cell composed of these components had a very high rate capacity of 718 mAh $\rm g^{-1}$ even at a relatively high charge density (4 C). After 200 cycles the cell still exhibited a capacity of 822 mAh $\rm g^{-1}$ (0.2 C). Although this performance does not outpace some of the cobalt catalyst systems or some of the other systems discussed herein, the use of iron and zinc which could be reclaimed from existing technologies might be expected to increase the sustainability of systems employing these metals as catalysts of polysulfide adsorbents.

Inorganic species can also play a role in interlayers. One strategy to employ modifies carbon nanofiber interlayers employed nanofibers decorated with MnS sites [117]. When the MnS-nanofiber interlayer was employed in a battery having a sulfur loading of 2 mg cm $^{-2}$, the authors reported that the voltage can remain constant at 2.37 V for up to 150 h after 20 cycles. In addition to demonstrating stability of the device, the authors also discuss the temperature-dependent performance of the battery. The room temperature capacity could reach 714 mAh g $^{-1}$ (after 400 cycles, 1 C). At elevated temperature (55 °C) or low temperature (0 °C) the capacity was 894 mAh g $^{-1}$ and 853 mAh g $^{-1}$, respectively (100 cycles, 0.5 C). Most of the studies on Li-S batteries report performance near room temperature, and more studies like this one would be beneficial given that battery-powered devices are used over a range of conditions.

Although standard metal phosphides have been studied in some detail for their use in Li-S batteries, a recent study [118] provided a good demonstration of how the addition of a second metal to a preformed metal phosphide may lead to a phase transformation such that enhance performance may be attained (Figure 21). In this case, addition of ruthenium to molybdenum phosphide (MoP) led to a phase change to a putative Mo_4P_3 species. This new phase was more efficient in its electrocatalytic conversion of polysulfides. When a cell was fabricated using the ruthenium- Mo_4P_3 nanoparticles on carbon nanospheres, the cell had a high capacity of 1178 mAh g^{-1} (0.5 C) or 660 mAh g^{-1} (4 C). Even with high sulfur loading of up to 6.6 mg cm⁻² and after 50 cycles, the materials show areal capacity of 5.6 mAh cm⁻². Given the plethora of transition metal combinations and metal sulfides available, there is still much work to be done to assess all of the promising possibilities for their use in Li-S batteries.

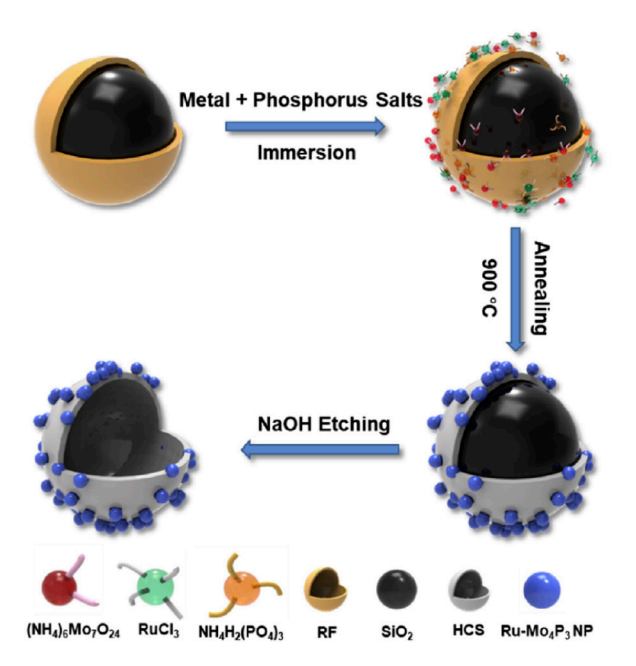


Figure 21. Stepwise assembly of spherical phosphide-containing shell materials on carbon nanospheres. Used with permission from reference [118], © 2020 used with permission from Elsevier.

4.8. Incorporation of Thiols and Organosulfur Compounds

Although there are many Li-S battery configurations making use of carbon nanotubes in their architecture, a recent report employing thiol-modified carbon nanotubes as the host material [119] is particularly intriguing because this material portends the possibility for the facile and reversible formation of new covalent S–S bonds between soluble species and the host material. The covalently-bound species would then be in close proximity to conductivity pathways provided by the carbon nanotubes. This configuration produced a cell that was able to maintain a capacity of 669.2 mAh $\rm g^{-1}$ even after 300 cycles (capacity fading rate of 0.166%/cycle, 0.1 C). This is about twice the capacity possible with a cell fabricated identically but with carbon nanotubes that are not modified with thiols (328.3 mAh $\rm g^{-1}$). Given the striking improvement in cell performance, other thiol-modified materials or other functional group modifications capable of reversible covalent bonding with sulfur species should be explored.

In another report the authors use organosulfur species to modify the cathode. The authors explore three specific organosulfur compounds having different electron-donating or electron-withdrawing characteristics: 3,5-bis(trifluoromethyl)phenyl thiol (BTF), diphenylsulfide (DPS), and bis(2-ethylenedioxyethyl) thiol (BDO) [120]. A dependence of the reduction voltage was noted to be BTF > $S_8 \sim DPS > BDO$. The catholyte utility of S of the cathode was increased by 28–49% upon addition of the organosulfur compounds, with the greatest increase coming when BDO was used as the additive. The authors explain these trends in terms of the electron-donating/-withdrawing ability of the organosulfur species and the increase in S utilization certainly suggests that the addition of organosulfur compounds is a viable strategy. Many more organosulfur additives should be surveyed to fully flesh out the structure–property relationships in these systems, however, as solubility and morphological distribution of the compounds within the cathode will also surely play a role.

4.9. Rational Design of Catalysts and Hybrid Systems

The rational design of catalysts has been a long-pursued dream in all areas of chemistry wherein catalysts are used. A recent approach to rationally design catalysts for Li-S batteries has been disclosed in the form of a "d-band tuning strategy", where the d-band refers to energies of d-electrons in a metallic material [78]. Tuning these energies was accomplished by methodically altering the composition of

cobalt alloys with nickel phosphide (Ni_2P). Addition of the Ni_2P increases interaction with polysulfides and in this study additional activity of species identified as $Ni_2Co_4P_3$ was delineated. Specifically, $Ni_2Co_4P_3$ species weaken the S–S bonds in bound polysulfides, thus catalyzing polysulfides conversion. This activity was monitored and confirmed by kinetic studies. Having confirmed the heightened activity of $Ni_2Co_4P_3$, the authors fabricated nanowires and composed a mat of these fibers on a nickel support to provide a large surface area, active catalytic material. An exceedingly high S loading of 25 mg cm⁻² was achieved in a "microreactor-like sulfur cathode" (MLSC). The MLSC cell showed a high capacity 1223 mAh g⁻¹ (0.1 C). This study illustrates several advantageous approaches to improving Li-S battery performance. First, catalysts should be rationally designed and rely on a combination of experimental and theoretical efforts applied in a mutual feedback loop. Second, designing catalyst elements to maximize surface area will guarantee that less material is needed to achieve a given performance, thus improving the sustainability of the process. Finally, creative designs like the MLSC could be applied with some of the other strategies and improvements discussed herein to further evaluate its benefits.

5. Advances in High Sulfur-Content Material Synthesis

The future of Li-S batteries undoubtedly will be formed by some synergistic, optimal combination of cathode and separator technologies. The affordable and sustainable synthesis of high sulfur-content materials would seem to be the centerpiece of such future compositions. Efforts to recycle valuable Li-S battery components such as metals [79] and polymers [80] are also an important aspect that is underway. The ability to control the sulfur rank, sulfur allotropic distribution, and mechanical properties of organosulfur polymers are exceedingly attractive for tuning battery performance and attenuating the shuttle effect that has thus far continued to plague Li-S batteries. It was not until 2013 that inverse vulcanization was reported [63] revolutionizing the accessibility of predesigned architectures [81–83]. Inverse vulcanization has proven successful for a wide range of olefins [84,85,121–128], including sustainably-sourced olefins [129]. Indeed, this newfound tunability has set off a firestorm of activity among researchers for Li-S batteries, so much so that an extensive and insightful review specifically on inverse vulcanization-produced materials for Li-S batteries has been reported [95]. More recently, an exciting new mechanism for high sulfur-content materials, radical-induced aryl halide-sulfur polymerization (RASP) was reported. This mechanism expands the scope of organic monomers beyond the olefins required of inverse vulcanization to include aryl halides. The potential for high sulfur-content aromatic organic architectures produced by RASP as cathodic media for Li-S batteries has yet to be tested, but the potential is sure to be exploited in the near future.

6. Conclusions and Outlook

The studies summarized in this review give a snapshot of the emerging work on Li-S batteries as of early 2020. Most of the work that has been undertaken has focused on the cathode and attenuating polysulfide solubility, transport and reaction within the cells. These properties are all influenced significantly by the surface area and proximity of adsorption sites to conductive parts of the scaffolds and membranes employed. More work on characterizing these aspects of the materials should be undertaken in the future to improve understanding of the mechanisms in order to drive rational design of future systems. For example, the development of in situ transmission electron microscopy for atomic resolution in battery components [130] should lead to remarkable insights that were previously inaccessible. The provocative possibility for the incorporation of single lithium-ion conducting polymer electrolytes is also an innovative strategy that holds great potential [131,132]. Emerging materials that can be employed in these systems are enriched by the recent discovery/engineering of new allotropic forms of carbon and sulfur and of synthetic routes to prepare high sulfur-content materials (inverse vulcanization and RASP), and these routes should be leveraged for extensive study to evaluate their utility in Li-S battery contexts. Safety concerns also remain with Li-S batteries. These safety concerns can be addressed by improved anode and anode interface research to prevent dendrite growth. Another

avenue to improving safety is to devise more active solid state or gel electrolytes or aqueous variations of Li-S batteries. Finally, if emerging battery technologies are to find a central place in the burgeoning green economy, sustainably sourced components should continue to be actively pursued.

Author Contributions: The authors have all contributed to gathering information from the literature and writing the article. R.C.S. is responsible for obtaining funding for the project. All authors have read and agreed to the published version of the manuscript.

Funding: This research was funded by National Science Foundation grant number CHE-1708844.

Acknowledgments: The authors would like to thank the NSF for funding this work (CHE-1708844).

Conflicts of Interest: The authors declare no conflict of interest.

References

- 1. Yang, H.; Chen, J.; Yang, J.; Wang, J. Prospect of Sulfurized Pyrolyzed Poly(acrylonitrile) (S@pPAN) Cathode Materials for Rechargeable Lithium Batteries. *Angew. Chem.* **2019**, *132*, 7374–7386. [CrossRef]
- 2. Xu, J.; Lawson, T.; Fan, H.; Su, D.; Wang, G. Updated Metal Compounds (MOFs, -S, -OH, -N, -C) Used as Cathode Materials for Lithium-Sulfur Batteries. *Adv. Energy Mater.* **2018**, *8*, 1702607. [CrossRef]
- 3. Xu, G.-L.; Wang, Q.; Fang, J.-C.; Xu, Y.-F.; Li, J.-T.; Huang, L.; Sun, S.-G. Tuning the structure and property of nanostructured cathode materials of lithium ion and lithium sulfur batteries. *J. Mater. Chem. A Mater. Energy Sustain.* **2014**, *2*, 19941–19962. [CrossRef]
- 4. Su, D.; Zhou, D.; Wang, C.; Wang, G. Toward High Performance Lithium-Sulfur Batteries Based on Li₂S Cathodes and Beyond: Status, Challenges, and Perspectives. *Adv. Funct. Mater.* **2018**, *28*, 1800154. [CrossRef]
- 5. Rehman, S.; Khan, K.; Zhao, Y.; Hou, Y. Nanostructured cathode materials for lithium-sulfur batteries: Progress, challenges and perspectives. *J. Mater. Chem. A Mater. Energy Sustain.* **2017**, *5*, 3014–3038. [CrossRef]
- 6. Pope, M.A.; Aksay, I.A. Structural Design of Cathodes for Li-S Batteries. *Adv. Energy Mater.* **2015**, *5*, 1500124. [CrossRef]
- 7. Eftekhari, A.; Kim, D.-W. Cathode materials for lithium-sulfur batteries: A practical perspective. *J. Mater. Chem. A Mater. Energy Sustain.* **2017**, *5*, 17734–17776. [CrossRef]
- 8. Zhang, S.; Ueno, K.; Dokko, K.; Watanabe, M. Recent Advances in Electrolytes for Lithium-Sulfur Batteries. *Adv. Energy Mater.* **2015**, *5*, 1500117. [CrossRef]
- 9. Yu, X.; Manthiram, A. Electrode-Electrolyte Interfaces in Lithium-Sulfur Batteries with Liquid or Inorganic Solid Electrolytes. *Acc. Chem. Res.* **2017**, *50*, 2653–2660. [CrossRef]
- 10. Wang, L.; Ye, Y.; Chen, N.; Huang, Y.; Li, L.; Wu, F.; Chen, R. Development and Challenges of Functional Electrolytes for High-Performance Lithium-Sulfur Batteries. *Adv. Funct. Mater.* **2018**, *28*, 1800919. [CrossRef]
- 11. Kaiser, M.R.; Chou, S.; Liu, H.-K.; Dou, S.-X.; Wang, C.; Wang, J. Structure-Property Relationships of Organic Electrolytes and Their Effects on Li/S Battery Performance. *Adv. Mater. Weinh. Ger.* **2017**, 29, 1700449. [CrossRef] [PubMed]
- 12. Baskoro, F.; Wong, H.Q.; Yen, H.-J. Strategic Structural Design of a Gel Polymer Electrolyte toward a High Efficiency Lithium-Ion Battery. *ACS Appl. Energy Mater.* **2019**, 2, 3937–3971. [CrossRef]
- 13. He, Y.; Chang, Z.; Wu, S.; Zhou, H. Effective strategies for long-cycle life lithium-sulfur batteries. J. Mater. Chem. A Mater. Energy Sustain. 2018, 6, 6155–6182. [CrossRef]
- 14. Zhao, Y.; Ye, Y.; Wu, F.; Li, Y.; Li, L.; Chen, R. Anode Interface Engineering and Architecture Design for High-Performance Lithium-Sulfur Batteries. *Adv. Mater. Weinh. Ger.* **2019**, *31*, 1806532. [CrossRef]
- 15. Tao, T.; Lu, S.; Fan, Y.; Lei, W.; Huang, S.; Chen, Y. Anode Improvement in Rechargeable Lithium-Sulfur Batteries. *Adv. Mater. Weinh. Ger.* **2017**, *29*, 1700542. [CrossRef]
- 16. Lin, D.; Liu, Y.; Cui, Y. Reviving the lithium metal anode for high-energy batteries. *Nat. Nanotechnol.* **2017**, 12, 194–206. [CrossRef]
- 17. Cao, R.; Xu, W.; Lv, D.; Xiao, J.; Zhang, J.-G. Anodes for Rechargeable Lithium-Sulfur Batteries. *Adv. Energy Mater.* **2015**, *5*, 1402273. [CrossRef]
- 18. Zhao, E.; Nie, K.; Yu, X.; Hu, Y.-S.; Wang, F.; Xiao, J.; Li, H.; Huang, X. Advanced Characterization Techniques in Promoting Mechanism Understanding for Lithium-Sulfur Batteries. *Adv. Funct. Mater.* **2018**, *28*, 1707543. [CrossRef]

19. Yan, Y.; Cheng, C.; Zhang, L.; Li, Y.-G.; Lu, J. Deciphering the Reaction Mechanism of Lithium–Sulfur Batteries by In Situ/Operando Synchrotron-Based Characterization Techniques. *Adv. Energy Mater.* **2019**, *9*. [CrossRef]

- Xu, R.; Lu, J.; Amine, K. Progress in Mechanistic Understanding and Characterization Techniques of Li-S Batteries. Adv. Energy Mater. 2015, 5, 1500408. [CrossRef]
- 21. Yue, J.; Yan, M.; Yin, Y.-X.; Guo, Y. Progress of the Interface Design in All-Solid-State Li-S Batteries. *Adv. Funct. Mater.* **2018**, *28*, 1707533. [CrossRef]
- 22. Liu, Y.; He, P.; Zhou, H. Rechargeable Solid-State Li-Air and Li-S Batteries: Materials, Construction, and Challenges. *Adv. Energy Mater.* **2017**, *8*, 1701602. [CrossRef]
- 23. Lin, Z.; Liang, C. Lithium–sulfur batteries: From liquid to solid cells. *J. Mater. Chem. A* **2015**, *3*, 936–958. [CrossRef]
- 24. Lei, D.; Shi, K.; Ye, H.; Wan, Z.; Wang, Y.; Shen, L.; Li, B.; Yang, Q.-H.; Kang, F.; He, Y.-B. Progress and Perspective of Solid-State Lithium-Sulfur Batteries. *Adv. Funct. Mater.* **2018**, *28*, 1707570. [CrossRef]
- 25. Yun, S.; Park, S.H.; Yeon, J.S.; Park, J.; Jana, M.; Suk, J.; Park, H.S. Materials and Device Constructions for Aqueous Lithium-Sulfur Batteries. *Adv. Funct. Mater.* **2018**, 28. [CrossRef]
- 26. Balach, J.; Linnemann, J.; Jaumann, T.; Giebeler, L. Metal-based nanostructured materials for advanced lithium-sulfur batteries. *J. Mater. Chem. A Mater. Energy Sustain.* **2018**, *6*, 23127–23168. [CrossRef]
- 27. Yuan, H.; Huang, J.-Q.; Peng, H.-J.; Titirici, M.-M.; Xiang, R.; Chen, R.; Liu, Q.; Zhang, Q. A Review of Functional Binders in Lithium-Sulfur Batteries. *Adv. Energy Mater.* **2018**, *8*. [CrossRef]
- 28. Xiang, Y.; Lia, J.; Lei, J.; Liu, D.; Xie, Z.; Qu, D.; Li, K.; Deng, T.; Tang, H. Advanced Separators for Lithium-Ion and Lithium-Sulfur Batteries: A Review of Recent Progress. *ChemSusChem* **2016**, *9*, 3023–3039. [CrossRef]
- 29. Ely, T.O.; Kamzabek, D.; Chakraborty, D.; Doherty, M.F. Lithium–Sulfur Batteries: State of the Art and Future Directions. *ACS Appl. Energy Mater.* **2018**, *1*, 1783–1814. [CrossRef]
- 30. Lochala, J.; Liu, D.; Wu, B.; Robinson, C.; Xiao, J. Research Progress toward the Practical Applications of Lithium–Sulfur Batteries. *ACS Appl. Mater. Interfaces* **2017**, *9*, 24407–24421. [CrossRef]
- 31. Li, X.; Sun, X. Interface Design and Development of Coating Materials in Lithium-Sulfur Batteries. *Adv. Funct. Mater.* **2018**, 28. [CrossRef]
- 32. Kumar, R.; Liu, J.; Hwang, J.-Y.; Sun, Y.-K. Recent research trends in Li–S batteries. *J. Mater. Chem. A* **2018**, 6, 11582–11605. [CrossRef]
- 33. Jeong, Y.C.; Kim, J.H.; Nam, S.; Park, C.R.; Yang, S.J. Rational Design of Nanostructured Functional Interlayer/Separator for Advanced Li-S Batteries. *Adv. Funct. Mater.* **2018**, *28*, 1707411. [CrossRef]
- 34. Guo, Q.; Zheng, Z. Rational Design of Binders for Stable Li-S and Na-S Batteries. *Adv. Funct. Mater.* **2019**, 30, 1907931. [CrossRef]
- 35. Fang, R.; Zhao, S.; Sun, Z.; Li, F.; Wang, D.-W.; Cheng, H.-M. More Reliable Lithium-Sulfur Batteries: Status, Solutions and Prospects. *Adv. Mater.* **2017**, 29, 1606823. [CrossRef] [PubMed]
- 36. Zheng, Y.; Zheng, S.; Xue, H.; Pang, H. Metal–organic frameworks for lithium–sulfur batteries. *J. Mater. Chem. A* **2019**, 7, 3469–3491. [CrossRef]
- 37. Liang, Z.; Qu, C.; Guo, W.; Zou, R.; Xu, Q. Pristine Metal-Organic Frameworks and their Composites for Energy Storage and Conversion. *Adv. Mater.* **2017**, *30*, 1702891. [CrossRef]
- 38. Yuan, H.; Liu, T.; Liu, Y.; Nai, J.; Wang, Y.; Zhang, W.; Tao, X. A review of biomass materials for advanced lithium–sulfur batteries. *Chem. Sci.* **2019**, *10*, 7484–7495. [CrossRef]
- 39. Wang, J.; Nie, P.; Ding, B.; Dong, S.; Hao, X.; Dou, H.; Zhang, X. Biomass derived carbon for energy storage devices. *J. Mater. Chem. A* **2017**, *5*, 2411–2428. [CrossRef]
- 40. Lim, W.-G.; Kim, S.; Jo, C.; Lee, J. A Comprehensive Review of Materials with Catalytic Effects in Li–S Batteries: Enhanced Redox Kinetics. *Angew. Chem. Int. Ed.* **2019**, *58*, 18746–18757. [CrossRef]
- 41. He, Y.; Zhang, Y.; Ding, F.; Li, X.; Wang, Z.; Lü, Z.; Wang, X.; Liu, Z.; Huang, X. Formation of hollow nanofiber rolls through controllable carbon diffusion for Li metal host. *Carbon* **2020**, *157*, 622–630. [CrossRef]
- 42. He, J.; Manthiram, A. Long-Life, High-Rate Lithium–Sulfur Cells with a Carbon-Free VN Host as an Efficient Polysulfide Adsorbent and Lithium Dendrite Inhibitor. *Adv. Energy Mater.* **2019**, *10*, 1903241. [CrossRef]
- 43. Li, S.; Ma, J.; Zeng, Z.; Hu, W.; Zhang, W.; Cheng, S.; Xie, J. Enhancing the kinetics of lithium–sulfur batteries under solid-state conversion by using tellurium as a eutectic accelerator. *J. Mater. Chem. A* **2020**, *8*, 3405–3412. [CrossRef]

44. Guo, R.; Zhang, S.; Wang, J.; Ying, H.; Han, W.-Q. One-Pot Synthesis of a Copolymer Micelle Crosslinked Binder with Multiple Lithium-Ion Diffusion Pathways for Lithium-Sulfur Batteries. *ChemSusChem* **2020**, 13, 819–826. [CrossRef] [PubMed]

- 45. Cui, J.; Li, Z.; Li, J.; Li, S.; Liu, J.; Shao, M.; Wei, M. An atomic-confined-space separator for high performance lithium–sulfur batteries. *J. Mater. Chem. A* **2020**, *8*, 1896–1903. [CrossRef]
- Li, Y.; Wang, C.; Wang, W.; Eng, A.Y.S.; Wan, M.; Fu, L.; Mao, E.; Li, G.; Tang, J.; Seh, Z.W.; et al. Enhanced Chemical Immobilization and Catalytic Conversion of Polysulfide Intermediates Using Metallic Mo Nanoclusters for High-Performance Li–S Batteries. ACS Nano 2019, 14, 1148–1157. [CrossRef] [PubMed]
- 47. Chiochan, P.; Kosasang, S.; Ma, N.; Duangdangchote, S.; Suktha, P.; Sawangphruk, M. Confining Li₂S₆ catholyte in 3D graphene sponge with ultrahigh total pore volume and oxygen-containing groups for lithium-sulfur batteries. *Carbon* **2020**, *158*, 244–255. [CrossRef]
- 48. Shen, G.; Liu, Z.; Lu, A.; Duan, J.; Younus, H.A.; Deng, H.; Wang, X.; Zhang, S. Constructing a 3D compact sulfur host based on carbon-nanotube threaded defective Prussian blue nanocrystals for high performance lithium-sulfur batteries. *J. Mater. Chem. A* **2020**, *8*, 1154–1163. [CrossRef]
- 49. Lee, J.; Jeon, Y.; Oh, J.; Kim, M.; Lee, L.Y.S.; Piao, Y. γ-Fe₂O₃ nanoparticles anchored in MWCNT hybrids as efficient sulfur hosts for high-performance lithium-sulfur battery cathode. *J. Electroanal. Chem.* **2020**, 858, 113806. [CrossRef]
- 50. Yu, B.; Chen, Y.; Wang, Z.; Chen, D.; Wang, X.; Zhang, W.; He, J.; He, W. 1T-MoS₂ nanotubes wrapped with N-doped graphene as highly-efficient absorbent and electrocatalyst for Li–S batteries. *J. Power Sources* **2020**, 447, 227364. [CrossRef]
- 51. Yanilmaz, M.; Asiri, A.M.; Zhang, X. Centrifugally spun porous carbon microfibers as interlayer for Li–S batteries. *J. Mater. Sci.* **2019**, *55*, 3538–3548. [CrossRef]
- 52. Song, J.; Zheng, J.; Zhang, R.; Fu, S.; Zhu, C.; Feng, S.; McEwen, J.-S.; Du, D.; Li, X.; Lin, Y. Enhancing Chemical Interaction of Polysulfide and Carbon through Synergetic Nitrogen and Phosphorus Doping. *ACS Sustain. Chem. Eng.* **2019**, *8*, 806–813. [CrossRef]
- 53. Yang, J.; Zhao, S.-X.; Zeng, X.; Lu, Y.; Cao, G. Catalytic Interfaces-Enriched Hybrid Hollow Spheres Sulfur Host for Advanced Li–S Batteries. *Adv. Mater. Interfaces* **2019**, 7. [CrossRef]
- 54. Li, Z.; Xiao, Z.; Li, P.; Meng, X.; Wang, R. Enhanced Chemisorption and Catalytic Effects toward Polysulfides by Modulating Hollow Nanoarchitectures for Long-Life Lithium–Sulfur Batteries. *Small* **2019**, *16*, 1906114. [CrossRef] [PubMed]
- 55. Yu, Z.; Liu, M.; Guo, D.; Wang, J.; Chen, X.; Jin, H.; Yang, Z.; Wang, S.; Li, J.; Chen, X.; et al. Radially inwardly aligned hierarchical porous carbon for ultra-long-life lithium-sulfur batteries. *Angew. Chem.* **2020**, 59, 6406–6411. [CrossRef] [PubMed]
- 56. Shao, A.-H.; Zhang, Z.; Xiong, D.-G.; Yu, J.; Cai, J.-X.; Yang, Z.-Y. Facile Synthesis of a "Two-in-One" Sulfur Host Featuring Metallic-Cobalt-Embedded N-Doped Carbon Nanotubes for Efficient Lithium-Sulfur Batteries. *ACS Appl. Mater. Interfaces* **2020**, *12*, 5968–5978. [CrossRef] [PubMed]
- 57. Wang, Z.; Shen, J.; Ji, S.; Xu, X.; Zuo, S.; Liu, Z.; Zhang, D.; Hu, R.; Ouyang, L.; Liu, J.; et al. B,N Codoped Graphitic Nanotubes Loaded with Co Nanoparticles as Superior Sulfur Host for Advanced Li–S Batteries. *Small* **2020**, *16*, 1906634. [CrossRef]
- 58. Wu, Z.; Yuan, L.; Han, Q.; Lan, Y.; Zhou, Y.; Jiang, X.; Ouyang, X.; Zhu, J.; Wang, X.; Fua, Y. Phosphorous/oxygen co-doped mesoporous carbon bowls as sulfur host for high performance lithium-sulfur batteries. *J. Power Sources* **2020**, 450, 227658. [CrossRef]
- 59. Tian, Y.; Li, G.; Zhang, Y.; Luo, D.; Wang, X.; Zhao, Y.; Liu, H.; Ji, P.; Du, X.; Li, J.; et al. Low-Bandgap Se-Deficient Antimony Selenide as a Multifunctional Polysulfide Barrier toward High-Performance Lithium-Sulfur Batteries. *Adv. Mater.* **2019**, 32, e1904876. [CrossRef]
- 60. Susarla, S.; Puthirath, A.B.; Tsafack, T.; Salpekar, D.; Babu, G.; Ajayan, P.M. Atomic-Level Alloying of Sulfur and Selenium for Advanced Lithium Batteries. *ACS Appl. Mater. Interfaces* **2019**, *12*, 1005–1013. [CrossRef]
- 61. Wang, B.; Guo, W.; Fu, Y. Anodized Aluminum Oxide Separators with Aligned Channels for High-Performance Li–S Batteries. *ACS Appl. Mater. Interfaces* **2020**, *12*, 5831–5837. [CrossRef] [PubMed]
- 62. Wang, J.; Wang, K.; Yang, Z.; Li, X.; Gao, J.; He, J.; Wang, N.; Wang, H.; Zhang, Y.; Huang, C. Effective Stabilization of Long-Cycle Lithium–Sulfur Batteries Utilizing In Situ Prepared Graphdiyne-Modulated Separators. ACS Sustain. Chem. Eng. 2019, 8, 1741–1750. [CrossRef]

63. Chung, W.J.; Griebel, J.J.; Kim, E.T.; Yoon, H.; Simmonds, A.G.; Ji, H.J.; Dirlam, P.T.; Glass, R.S.; Wie, J.J.; Nguyen, N.A.; et al. The use of elemental sulfur as an alternative feedstock for polymeric materials. *Nat. Chem.* **2013**, *5*, 518–524. [CrossRef] [PubMed]

- 64. Zhang, Y.-J.; Liu, X.; Wu, L.; Dong, W.; Xia, F.-J.; Chen, L.-D.; Zhou, N.; Xia, L.; Hu, Z.-Y.; Liu, J.; et al. A flexible, hierarchically porous PANI/MnO2 network with fast channels and an extraordinary chemical process for stable fast-charging lithium–sulfur batteries. *J. Mater. Chem. A* **2020**, *8*, 2741–2751. [CrossRef]
- 65. Wei, W.; Li, J.; Wang, Q.; Liu, D.; Niu, J.; Liu, P. Hierarchically Porous SnO₂ Nanoparticle-Anchored Polypyrrole Nanotubes as a High-Efficient Sulfur/Polysulfide Trap for High-Performance Lithium–Sulfur Batteries. *ACS Appl. Mater. Interfaces* **2020**, *12*, 6362–6370. [CrossRef]
- 66. Chen, C.; Xu, H.; Zhang, B.; Jiang, Q.; Zhang, Y.; Li, L.; Lin, Z. Rational design of a mesoporous silica-based cathode for efficient trapping of polysulfides in Li-S batteries. *Chem. Commun.* **2020**, *56*, 786–789. [CrossRef]
- 67. Liu, X.; Chen, P.; Chen, J.; Zeng, Q.; Wang, Z.; Li, Z.; Zhang, L. A nitrogen-rich hyperbranched polymer as cathode encapsulated material for superior long-cycling lithium-sulfur batteries. *Electrochim. Acta* **2020**, *330*, 135337. [CrossRef]
- 68. Lin, J.; Zhang, K.; Zhu, Z.; Zhang, R.; Li, N.; Zhao, C. CoP/C Nanocubes-Modified Separator Suppressing Polysulfide Dissolution for High-Rate and Stable Lithium–Sulfur Batteries. *ACS Appl. Mater. Interfaces* **2019**, 12, 2497–2504. [CrossRef]
- 69. Chen, M.; Li, C.; Fu, X.; Wei, W.; Fan, X.; Hattori, A.; Chen, Z.; Liu, J.; Zhong, W.-H. Let It Catch: A Short-Branched Protein for Efficiently Capturing Polysulfides in Lithium–Sulfur Batteries. *Adv. Energy Mater.* **2020**, *10*. [CrossRef]
- 70. Wang, H.; Zhang, W.; Xu, J.; Guo, Z. Advances in Polar Materials for Lithium-Sulfur Batteries. *Adv. Funct. Mater.* **2018**, *28*. [CrossRef]
- 71. Wang, Y.; Yu, Y.; Tan, Y.; Li, T.; Chen, Y.; Wang, S.; Sui, K.; Zhang, H.; Luo, Y.; Li, X. Affinity Laminated Chromatography Membrane Built-in Electrodes for Suppressing Polysulfide Shuttling in Lithium–Sulfur Batteries. *Adv. Energy Mater.* **2019**, *10*, 1903233. [CrossRef]
- 72. Zuoab, Y.; Zhao, M.; Ren, P.; Suab, W.; Zhou, J.; Chen, Y.; Tang, Y.; Chen, Y. An efficient polysulfide trapper of an nitrogen and nickel-decorating amylum scaffold-coated separator for ultrahigh performance in lithium–sulfur batteries. *J. Mater. Chem. A* **2020**, *8*, 1238–1246. [CrossRef]
- 73. Li, G.; Lu, F.; Dou, X.; Wang, X.; Luo, D.; Sun, H.; Yu, A.; Chen, Z. Polysulfide Regulation by the Zwitterionic Barrier toward Durable Lithium–Sulfur Batteries. *J. Am. Chem. Soc.* **2020**, *142*, 3583–3592. [CrossRef]
- 74. Li, B.; Xie, M.; Yi, G.; Zhang, C. Biomass-derived activated carbon/sulfur composites as cathode electrodes for Li–S batteries by reducing the oxygen content. *RSC Adv.* **2020**, *10*, 2823–2829. [CrossRef]
- 75. Razzaq, A.A.; Yuan, X.; Chen, Y.; Hu, J.; Mu, Q.; Ma, Y.; Zhao, X.; Miao, L.; Ahn, J.-H.; Peng, Y.; et al. Anchoring MOF-derived CoS₂ on sulfurized polyacrylonitrile nanofibers for high areal capacity lithium–sulfur batteries. *J. Mater. Chem. A* **2020**, *8*, 1298–1306. [CrossRef]
- 76. Xu, W.; Pang, H.; Zhou, H.; Jian, Z.; Hu, R.; Xing, Y.; Zhang, S. Lychee-like TiO₂@TiN dual-function composite material for lithium–sulfur batteries. *RSC Adv.* **2020**, *10*, 2670–2676. [CrossRef]
- 77. Chen, P.; Wang, Z.; Zhang, B.; Liu, H.; Liu, W.; Zhao, J.; Ma, Z.; Dong, W.; Su, Z. Reduced graphene oxide/TiO₂(B) nanocomposite-modified separator as an efficient inhibitor of polysulfide shuttling in Li–S batteries. *RSC Adv.* **2020**, *10*, 4538–4544. [CrossRef]
- 78. Shen, Z.; Cao, M.; Zhang, Z.; Pu, J.; Zhong, C.; Li, J.; Ma, H.; Li, F.; Zhu, J.; Pan, F.; et al. Efficient Ni 2 Co 4 P 3 Nanowires Catalysts Enhance Ultrahigh-Loading Lithium–Sulfur Conversion in a Microreactor-Like Battery. *Adv. Funct. Mater.* **2019**, *30.* [CrossRef]
- 79. Yang, Y.; Lei, S.; Song, S.; Sun, W.; Wang, L. Stepwise recycling of valuable metals from Ni-rich cathode material of spent lithium-ion batteries. *Waste Manag.* **2020**, *102*, 131–138. [CrossRef]
- 80. Thiounn, T.; Smith, R.C. Advances and approaches for chemical recycling of plastic waste. *J. Appl. Polym. Sci.* **2020**, *58*, 1347–1364. [CrossRef]
- 81. Chalker, J.M.; Worthington, M.J.H.; Lundquist, N.A.; Esdaile, L.J. Synthesis and Applications of Polymers Made by Inverse Vulcanization. *Top. Curr. Chem.* **2019**, *377*, 16. [CrossRef] [PubMed]
- 82. Lim, J.; Pyun, J.; Char, K. Recent Approaches for the Direct Use of Elemental Sulfur in the Synthesis and Processing of Advanced Materials. *Angew. Chem. Int. Ed.* **2015**, *54*, 3249–3258. [CrossRef] [PubMed]

83. Zhang, Y.; Glass, R.S.; Char, K.; Pyun, J.; Pyun, J. Recent advances in the polymerization of elemental sulphur, inverse vulcanization and methods to obtain functional Chalcogenide Hybrid Inorganic/Organic Polymers (CHIPs). *Polym. Chem.* **2019**, *10*, 4078–4105. [CrossRef]

- 84. Smith, A.D.; Smith, R.C.; Tennyson, A.G. Carbon-Negative Polymer Cements by Copolymerization of Waste Sulfur, Oleic Acid, and Pozzolan Cements. *Sustain. Chem. Pharm.* **2020**, *16*, 100249. [CrossRef]
- 85. Karunarathna, M.; Smith, R.C. Valorization of Lignin as a Sustainable Component of Structural Materials and Composites: Advances from 2011 to 2019. *Sustainability* **2020**, *12*, 734. [CrossRef]
- 86. Tang, B.; Wu, H.; Du, X.; Cheng, X.; Liu, X.; Yu, Z.; Yang, J.; Zhang, M.; Zhang, J.; Cui, G. Highly Safe Electrolyte Enabled via Controllable Polysulfide Release and Efficient Conversion for Advanced Lithium–Sulfur Batteries. *Small* **2020**, *16*, e1905737. [CrossRef]
- 87. E Camacho-Forero, L.; Balbuena, P.B. Elucidating Interfacial Phenomena between Solid-State Electrolytes and the Sulfur-Cathode of Lithium-Sulfur Batteries. *ECS Meet. Abstr.* **2019**, *32*, 360–373. [CrossRef]
- 88. Xiao, Q.; Deng, C.; Wang, Q.; Zhang, Q.; Yue, Y.; Ren, S. In Situ Cross-Linked Gel Polymer Electrolyte Membranes with Excellent Thermal Stability for Lithium Ion Batteries. *ACS Omega* **2019**, *4*, 95–103, Available online: https://pubs.acs.org/doi/full/10.1021/acsomega.8b02255 (accessed on 10 June 2020). [CrossRef]
- 89. Baik, S.; Park, J.H.; Lee, J.W. One-pot conversion of carbon dioxide to CNT-grafted graphene bifunctional for sulfur cathode and thin interlayer of Li–S battery. *Electrochim. Acta* **2020**, *330*, 135264. [CrossRef]
- 90. Shi, H.; Lv, W.; Zhang, C.; Wang, D.-W.; Ling, G.; He, Y.-B.; Kang, F.; Yang, Q.-H. Functional Carbons Remedy the Shuttling of Polysulfides in Lithium-Sulfur Batteries: Confining, Trapping, Blocking, and Breaking up. *Adv. Funct. Mater.* **2018**, *28*. [CrossRef]
- 91. Kensy, C.; Härtel, P.; Maschita, J.; Dörfler, S.; Schumm, B.; Abendroth, T.; Althues, H.; Lotsch, B.V.; Kaskel, S. Scalable production of nitrogen-doped carbons for multilayer lithium-sulfur battery cells. *Carbon* **2020**, *161*, 190–197. [CrossRef]
- 92. Shih, H.-J.; Chang, J.-Y.; Cho, C.-S.; Li, C.-C. Nano-carbon-fiber-penetrated sulfur crystals as potential cathode active material for high-performance lithium–sulfur batteries. *Carbon* **2020**, *159*, 401–411. [CrossRef]
- 93. Liu, N.; Zhou, G.; Yang, A.; Yu, X.; Shi, F.; Sun, J.; Zhang, J.; Liu, B.; Wu, C.-L.; Tao, X.; et al. Direct electrochemical generation of supercooled sulfur microdroplets well below their melting temperature. *Proc. Natl. Acad. Sci. USA* **2019**, *116*, 765–770. [CrossRef] [PubMed]
- 94. Yang, A.; Zhou, G.; Kong, X.; Vilá, R.A.; Pei, A.; Wu, Y.; Yu, X.; Zheng, X.; Wu, C.-L.; Liu, B.; et al. Electrochemical generation of liquid and solid sulfur on two-dimensional layered materials with distinct areal capacities. *Nat. Nanotechnol.* **2020**, *15*, 231–237. [CrossRef] [PubMed]
- 95. Zhao, F.; Li, Y.; Feng, W. Recent Advances in Applying Vulcanization/Inverse Vulcanization Methods to Achieve High-Performance Sulfur-Containing Polymer Cathode Materials for Li-S Batteries. *Small Methods* **2018**, *2*, 1–34. [CrossRef]
- 96. Liu, X.; Lu, Y.; Zeng, Q.; Chen, P.; Li, Z.; Wen, X.; Wen, W.; Li, Z.; Zhang, L. Trapping of Polysulfides with Sulfur-Rich Poly Ionic Liquid Cathode Materials for Ultralong-Life Lithium–Sulfur Batteries. *ChemSusChem* **2020**, *13*, 715–723. [CrossRef]
- 97. He, Y.; Matthews, B.; Wang, J.; Song, L.; Wang, X.; Wu, G. Innovation and challenges in materials design for flexible rechargeable batteries: From 1D to 3D. *J. Mater. Chem. A* **2018**, *6*, 735–753. [CrossRef]
- 98. Peng, H.-J.; Huang, J.-Q.; Zhang, Q. A review of flexible lithium–sulfur and analogous alkali metal–chalcogen rechargeable batteries. *Chem. Soc. Rev.* **2017**, *46*, 5237–5288. [CrossRef]
- 99. Mukkabla, R.; Ojha, M.; Deepa, M. Poly(N-methylpyrrole) barrier coating and SiO2 fillers based gel electrolyte for safe and reversible Li–S batteries. *Electrochim. Acta* **2020**, *334*, 135571. [CrossRef]
- 100. Wei, Y.; Li, X.; Xu, Z.; Sun, H.; Zheng, Y.; Peng, L.; Liu, Z.; Gao, C.; Gao, M. Solution processible hyperbranched inverse-vulcanized polymers as new cathode materials in Li–S batteries. *Polym. Chem.* **2015**, *6*, 973–982. [CrossRef]
- 101. Hua, Z.; Sua, H.; Tua, S.; Xionga, P.; Chenga, M.; Zhaoa, X.; Wanga, L.; Zhua, Y.; Li, F.; Xu, Y. Efficient polysulfide trapping enabled by a polymer adsorbent in lithium-sulfur batteries. *Electrochim. Acta* **2020**, *336*, 135693. [CrossRef]
- 102. Zhong, Y.; Lin, F.; Wang, M.; Zhang, Y.; Ma, Q.; Lin, J.; Feng, Z.; Wang, H. Metal Organic Framework Derivative Improving Lithium Metal Anode Cycling. *Adv. Funct. Mater.* **2020**, *30*, 1907579. [CrossRef]
- 103. Wei, L.; Li, W.; Zhao, T.; Zhang, N.; Li, L.; Wu, F.; Chen, R. Cobalt nanoparticles shielded in N-doped carbon nanotubes for high areal capacity Li–S batteries. *Chem. Commun.* **2020**, *56*, 3007–3010. [CrossRef] [PubMed]

104. Yao, S.; Guo, R.; Xie, F.; Wu, Z.; Gao, K.; Zhang, C.; Shen, X.; Li, T.; Qin, S. Electrospun three-dimensional cobalt decorated nitrogen doped carbon nanofibers network as freestanding electrode for lithium/sulfur batteries. *Electrochim. Acta* **2020**, 337, 135765. [CrossRef]

- 105. Cai, J.; Song, Y.-Z.; Chen, X.; Sun, Z.; Yi, Y.; Sun, J.; Zhang, Q. MOF-derived conductive carbon nitrides for separator-modified Li–S batteries and flexible supercapacitors. *J. Mater. Chem. A* **2020**, *8*, 1757–1766. [CrossRef]
- 106. Wang, R.; Yang, J.; Chen, X.; Zhao, Y.; Zhao, W.; Qian, G.; Li, S.; Xiao, Y.; Chen, H.; Ye, Y.; et al. Highly Dispersed Cobalt Clusters in Nitrogen-Doped Porous Carbon Enable Multiple Effects for High-Performance Li–S Battery. *Adv. Energy Mater.* **2020**, *10*. [CrossRef]
- 107. Li, Y.; Lin, S.; Wang, D.; Gao, T.; Song, J.; Zhou, P.; Xu, Z.; Yang, Z.; Xiao, N.; Guo, S. Single Atom Array Mimic on Ultrathin MOF Nanosheets Boosts the Safety and Life of Lithium–Sulfur Batteries. *Adv. Mater.* **2020**, 32, e1906722. [CrossRef]
- 108. Jin, J.; Cai, W.; Cai, J.; Shao, Y.; Song, Y.-Z.; Xia, Z.; Zhang, Q.; Sun, J. MOF-derived hierarchical CoP nanoflakes anchored on vertically erected graphene scaffolds as self-supported and flexible hosts for lithium–sulfur batteries. *J. Mater. Chem. A* **2020**, *8*, 3027–3034. [CrossRef]
- 109. Wang, C.; Song, H.; Yu, C.; Ullah, Z.; Guan, Z.; Chu, R.; Zhang, Y.; Zhao, L.; Li, Q.; Liu, L. Iron single-atom catalyst anchored on nitrogen-rich MOF-derived carbon nanocage to accelerate polysulfide redox conversion for lithium sulfur batteries. *J. Mater. Chem. A* **2020**, *8*, 3421–3430. [CrossRef]
- 110. Chen, S.; Ming, Y.; Tan, B.; Chen, S. Carbon-free sulfur-based composite cathode for advanced Lithium-Sulfur batteries: A case study of hierarchical structured CoMn₂O₄ hollow microspheres as sulfur immobilizer. *Electrochim. Acta* **2020**, 329, 135128. [CrossRef]
- 111. Liu, H.; Chen, M.; Zeng, P.; Li, X.; Luo, J.; Li, Y.; Xing, T.; Chang, B.; Wang, X.; Luo, Z. Lithium Sulfide-Embedded Three-Dimensional Heterogeneous Micro-/Mesoporous Interwoven Carbon Architecture as the Cathode of Lithium-Sulfur Batteries. *ACS Sustain. Chem. Eng.* **2020**, *8*, 351–361. [CrossRef]
- 112. Liu, X.; Huang, J.-Q.; Zhang, Q.; Mai, L. Nanostructured Metal Oxides and Sulfides for Lithium-Sulfur Batteries. *Adv. Mater.* **2017**, *29*, 1601759. [CrossRef] [PubMed]
- 113. Li, Y.; Jiang, T.; Yang, H.; Lei, D.; Deng, X.; Hao, C.; Zhang, F.; Guo, J. A heterostuctured Co₃S₄/MnS nanotube array as a catalytic sulfur host for lithium-sulfur batteries. *Electrochim. Acta* **2020**, 330, 135311. [CrossRef]
- 114. Guo, D.; Zhang, Z.; Xi, B.; Yu, Z.; Zhou, Z.; Chen, X. Ni₃S₂ Anchored into N/S co-doped Reduced Graphene Oxide with Highly Pleated Structure as a Sulfur Host for Lithium-Sulfur Batteries. *J. Mater. Chem. A Mater. Energy Sustain.* 2020, *8*, 3834–3844. [CrossRef]
- 115. Zhou, L.; Zhuang, Z.; Zhao, H.; Lin, M.; Zhao, D.; Mai, L. Intricate Hollow Structures: Controlled Synthesis and Applications in Energy Storage and Conversion. *Adv. Mater.* **2017**, *29*, 1602914. [CrossRef]
- 116. Li, W.; Gong, Z.; Yan, X.; Wang, D.; Liu, J.; Guo, X.; Zhang, Z.; Li, G. In situ engineered ZnS–FeS heterostructures in N-doped carbon nanocages accelerating polysulfide redox kinetics for lithium sulfur batteries. *J. Mater. Chem. A* **2020**, *8*, 433–442. [CrossRef]
- 117. Wang, X.; Zhao, X.; Ma, C.; Yang, Z.; Chen, G.; Wang, L.; Yue, H.; Zhang, D.; Sun, Z. Electrospun carbon nanofibers with MnS sulfiphilic sites as efficient polysulfide barriers for high-performance wide-temperature-range Li–S batteries. *J. Mater. Chem. A* 2020, *8*, 1212–1220. [CrossRef]
- 118. Ma, F.; Wang, X.; Wang, J.; Tian, Y.; Liang, J.; Fan, Y.; Wang, L.; Wang, T.; Cao, R.; Jiao, S.; et al. Phase-transformed Mo₄P₃ nanoparticles as efficient catalysts towards lithium polysulfide conversion for lithium–sulfur battery. *Electrochim. Acta* **2020**, *330*, 135310. [CrossRef]
- 119. Xu, Y.-W.; Zhang, B.-H.; Li, G.-R.; Liu, S.; Gao, X.-P. Covalently Bonded Sulfur Anchored with Thiol-Modified Carbon Nanotube as a Cathode Material for Lithium–Sulfur Batteries. *ACS Appl. Energy Mater.* **2019**, *3*, 487–494. [CrossRef]
- 120. Phadke, S.; Pires, J.; Korchenko, A.; Anouti, M. How do organic polysulphides improve the performance of Li-S batteries? *Electrochim. Acta* **2020**, *330*, 135253. [CrossRef]
- 121. Smith, A.D.; McMillen, C.D.; Smith, R.C.; Tennyson, A.G. Copolymers by Inverse Vulcanization of Sulfur with Pure or Technical-Grade Unsaturated Fatty Acids. *J. Appl. Polym. Sci.* **2020**, *58*, 438–445. [CrossRef]
- 122. Karunarathna, M.S.; Tennyson, A.G.; Smith, R.C. Facile new approach to high sulfur-content materials and preparation of sulfur-lignin copolymers. *J. Mater. Chem. A* **2020**, *8*, 548–553. [CrossRef]
- 123. Karunarathna, M.S.; Lauer, M.K.; Tennyson, A.G.; Smith, R.C. Copolymerization of an aryl halide and elemental sulfur as a route to high sulfur content materials. *Polym. Chem.* **2020**, *11*, 1621–1628. [CrossRef]

124. Thiounn, T.; Tennyson, A.G.; Smith, R.C. Durable, acid-resistant copolymers from industrial by-product sulfur and microbially-produced tyrosine. *RSC Adv.* **2019**, *9*, 31460–31465. [CrossRef]

- 125. Smith, A.D.; Thiounn, T.; Lyles, E.W.; Kibler, E.K.; Smith, R.C.; Tennyson, A.G. Combining agriculture and energy industry waste products to yield recyclable, thermally healable copolymers of elemental sulfur and oleic acid. *J. Polym. Sci. Part A Polym. Chem.* **2019**, *57*, 1704–1710. [CrossRef]
- 126. Lauer, M.K.; Estrada-Mendoza, T.A.; McMillen, C.D.; Chumanov, G.; Tennyson, A.G.; Smith, R.C. Durable Cellulose–Sulfur Composites Derived from Agricultural and Petrochemical Waste. *Adv. Sustain. Syst.* **2019**, 3, 1900062. [CrossRef]
- 127. Karunarathna, M.S.; Lauer, M.K.; Thiounn, T.; Smith, R.C.; Tennyson, A.G. Valorization of waste to yield recyclable composites of elemental sulfur and lignin. *J. Mater. Chem. A Mater. Energy Sustain.* **2019**, 7, 15683–15690. [CrossRef]
- 128. Thiounn, T.; Lauer, M.K.; Bedford, M.S.; Smith, R.C.; Tennyson, A.G. Thermally-healable network solids of sulfur-crosslinked poly(4-allyloxystyrene). *RSC Adv.* **2018**, *8*, 39074–39082. [CrossRef]
- 129. Worthington, M.J.H.; Kucera, R.L.; Chalker, J.M. Green chemistry and polymers made from sulfur. *Green Chem.* **2017**, *19*, 2748–2761. [CrossRef]
- 130. Zhang, C.; Firestein, K.L.; Fernando, J.F.S.; Siriwardena, D.; Von Treifeldt, J.; Golberg, D. Recent Progress of In Situ Transmission Electron Microscopy for Energy Materials. *Adv. Mater.* **2019**, 32, e1904094. [CrossRef]
- 131. Nicotera, I.; Simari, C.; Agostini, M.; Enotiadis, A.; Brutti, S. A Novel Li+-Nafion-Sulfonated Graphene Oxide Membrane as Single Lithium-Ion Conducting Polymer Electrolyte for Lithium Batteries. *J. Phys. Chem. C* **2019**, 123, 27406–27416. [CrossRef]
- 132. Jin, Z.-Q.; Xie, K.; Hong, X.; Hu, Z.; Liu, X. Application of lithiated Nafion ionomer film as functional separator for lithium sulfur cells. *J. Power Sources* **2012**, *218*, 163–167. [CrossRef]



© 2020 by the authors. Licensee MDPI, Basel, Switzerland. This article is an open access article distributed under the terms and conditions of the Creative Commons Attribution (CC BY) license (http://creativecommons.org/licenses/by/4.0/).